HYPK controls stability and catalytic activity of the N-terminal acetyltransferase A in Arabidopsis thaliana

Xiaodi Gong, Jean-Baptiste Boyer, Simone Gierlich, Marlena Pożoga, Jonas Weidenhausen, Irmgard Sinning, Thierry Meinnel, Carmela Giglione, Yonghong Wang, Rüdiger Hell, et al.

Cell Reports

Article

HYPK controls stability and catalytic activity of the N-terminal acetyltransferase A in *Arabidopsis thaliana*

Graphical abstract

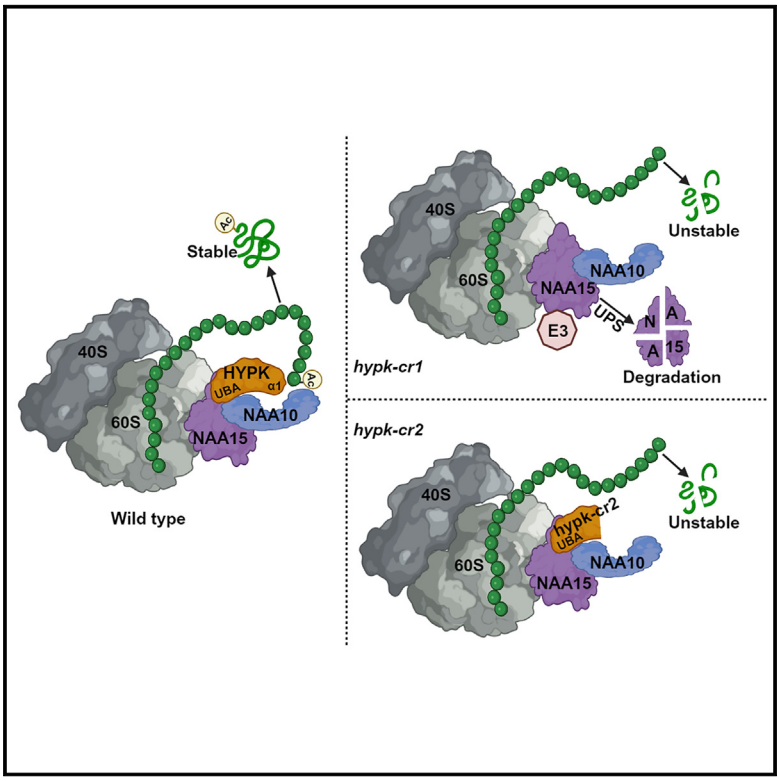

Highlights

- The UBA domain of HYPK stabilizes NAA15 *in planta* in an organ-specific manner
- Helix α1 of HYPK is critical for the maintenance of NatA activity in plants
- Helix α1 must be correctly positioned at the NatA complex by UBA domain to fulfill its function

Authors

Xiaodi Gong, Jean-Baptiste Boyer, Simone Gierlich, ..., Yonghong Wang, Rüdiger Hell, Markus Wirtz

Correspondence

markus.wirtz@cos.uni-heidelberg.de

In brief

Gong et al. find that drought tolerance and proteome stability in the reference plant *Arabidopsis thaliana* depend on helix α1 and the UBA domain of HYPK. HYPK binds to the co-translationally acting N-terminal acetyltransferase A and controls its stability and activity in an organ-specific manner.

Gong et al., 2024, Cell Reports *43*, 113768
February 27, 2024
https://doi.org/10.1016/j.celrep.2024.113768

CellPress

Cell Reports

CellPress
OPEN ACCESS

Article

HYPK controls stability and catalytic activity of the N-terminal acetyltransferase A in *Arabidopsis thaliana*

Xiaodi Gong,[1] Jean-Baptiste Boyer,[2] Simone Gierlich,[1] Marlena Pożoga,[1] Jonas Weidenhausen,[3] Irmgard Sinning,[3] Thierry Meinnel,[2] Carmela Giglione,[2] Yonghong Wang,[4] Rüdiger Hell,[1] and Markus Wirtz[1,5,*]

[1]Centre for Organismal Studies, Heidelberg University, 69120 Heidelberg, Germany
[2]Université Paris-Saclay, CEA, CNRS, Institute for Integrative Biology of the Cell (I2BC), 91198 Gif-sur-Yvette, France
[3]Heidelberg University Biochemistry Center, 69120 Heidelberg, Germany
[4]State Key Laboratory of Crop Biology, College of Life Sciences, Shandong Agricultural University, 271018 Tai'an, China
[5]Lead contact
*Correspondence: markus.wirtz@cos.uni-heidelberg.de
https://doi.org/10.1016/j.celrep.2024.113768

SUMMARY

The ribosome-tethered N-terminal acetyltransferase A (NatA) acetylates 52% of soluble proteins in *Arabidopsis thaliana*. This co-translational modification of the N terminus stabilizes diverse cytosolic plant proteins. The evolutionary conserved Huntingtin yeast partner K (HYPK) facilitates NatA activity *in planta*, but *in vitro*, its N-terminal helix α1 inhibits human NatA activity. To dissect the regulatory function of HYPK protein domains *in vivo*, we genetically engineer CRISPR-Cas9 mutants expressing a HYPK fragment lacking all functional domains (*hypk-cr1*) or an internally deleted HYPK variant truncating helix α1 but retaining the C-terminal ubiquitin-associated (UBA) domain (*hypk-cr2*). We find that the UBA domain of HYPK is vital for stabilizing the NatA complex in an organ-specific manner. The N terminus of HYPK, including helix α1, is critical for promoting NatA activity on substrates starting with various amino acids. Consequently, deleting only 42 amino acids inside the HYPK N terminus causes substantial destabilization of the plant proteome and higher tolerance toward drought stress.

INTRODUCTION

N^{α}-terminal acetylation (NTA) is a prevalent protein modification experimentally found on approximately 80% of proteins in humans, *Drosophila*, and *Arabidopsis*.[1–3] In animals, the bulk of proteins are imprinted co-translationally with acetylation marks by ribosome-associated N-acetyltransferases (Nats). The cytosolic N-acetylation machinery consists of six Nats termed NatA to NatF, which are conserved in multicellular eukaryotes.[4,5] Each Nat complex comprises at least one catalytic and up to two auxiliary subunits.[2] The substrate specificity of the ribosome-associated Nats is narrow and mainly defined by their substrate proteins' first two amino acids.[6–8] On top of these Nats, plants possess additional protein acetylation machinery in plastids (NatG) and the plasma membrane (NatF) with a more relaxed substrate specificity.[4,9–12]

The NatA is the most promiscuous Nat in all eukaryotes and targets the N termini of proteins undergoing initiator methionine (iMet) removal by methionine aminopeptidase (MetAP). Approximately 40% of plant proteins are predicted to be a substrate of NatA, resulting in acetylated N termini starting with small amino acids such as Ser, Gly, Ala, Thr, and Cys.[13] The high number of predicted NatA substrates is corroborated by global N-terminome profiling of leaf proteins, uncovering that 52% of detected soluble leaf proteins are N-terminally acetylated NatA substrates, as reviewed in Pożoga et al.[8] and Meinnel and Giglionne.[13] However, not all NatA substrates are entirely acetylated at their N terminus, suggesting precise and complicated regulatory mechanisms controlling the NTA frequency of NatA substrates. The core NatA complex comprises the catalytic subunit NAA10 and the ribosome anchoring subunit NAA15. Both core NatA subunits are essential in plants since the absence of one core subunit results in embryo lethality at the globular state.[14] Depletion of NatA activity in plants severely retards growth but, at the same time, enhances resilience against pathogens and drought stress.[14,15] Also, other plant Nats have been linked to adaptation toward biotic and abiotic inputs.[4,16,17]

The dynamic plasticity of the plant proteome is crucial to cope with such environmental stresses. One critical stress-responsive mechanism to rapidly adjust the abundance of a protein is to regulate its degradation rate by the ubiquitin-proteasome system (UPS).[18] Besides many other functions,[6] NTA can control the stability of proteins by creating or masking N-terminally encoded degradation signals (N-degrons) that are recognized in humans and fungi by E3 ligases (N-recognins).[19–22] Several examples demonstrate that stress-related proteins like the immune receptor SNC1 and the SIGMA factor binding protein 1 are also regulated in their stability by NTA.[15,23] In plants, NTA stabilizes

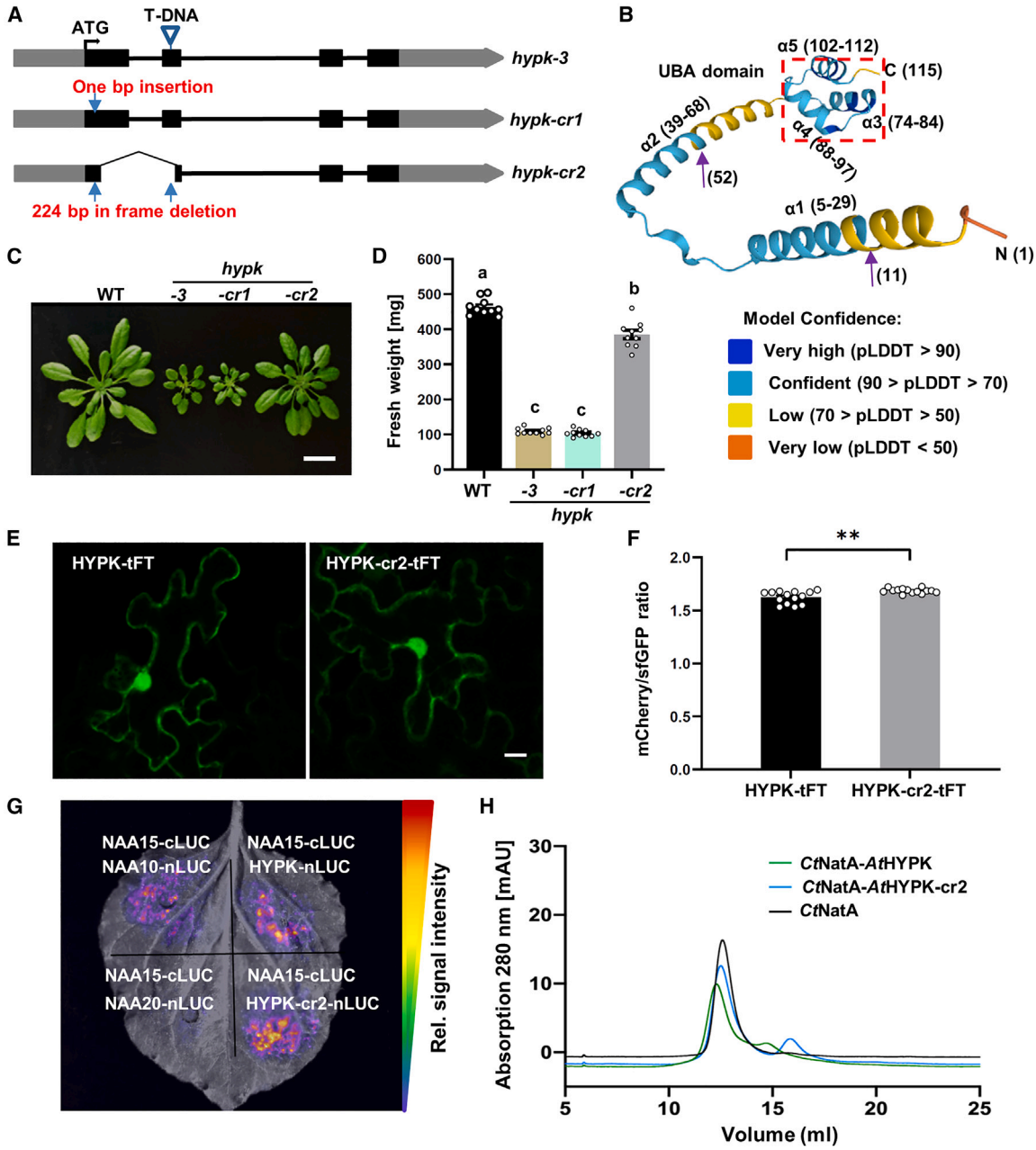

Figure 1. Identification and characterization of the *hypk-cr* mutants

(A) Schematic representation of mutations in the *HYPK* gene of the transfer DNA insertion mutant, *hypk-3*, and the novel CRISPR-Cas9 genome-editing mutants, *hypk-cr1* and *hypk-cr2*. Gray boxes indicate 5′ UTR, black boxes represent exons, and introns and 3′ UTRs are shown as lines or gray arrows, respectively.

(B) Prediction of *At*HYPK structure by AlphaFold.[43] Arrows indicate the 42 amino acids deleted in the N terminus of the HYPK-cr2 protein. Color coding indicates the confidence level of the model as defined in the legend. The red box highlights the UBA domain forming a triple-helix bundle.

(C and D) Phenotype (C) and fresh weight (D) of 6-week-old soil-grown wild-type (WT), *hypk-3*, *hypk-cr1*, and *hypk-cr2* plants. Data are shown as means ± SEM. Circles indicate individual data points. Different letters indicate individual groups identified by pairwise multiple comparisons with a one-way ANOVA followed by a Tukey's test ($p < 0.05$, $n = 10$). Scale bar: 2 cm.

(E) Subcellular localization of HYPK-tFT (tandem fluorescent timer) and HYPK-cr2-tFT fusion proteins in tobacco pavement cells as determined by the sfGFP signal of the tFT.[44] Scale bar: 20 μm.

(F) Relative protein half-life time of the HYPK-tFT and the HYPK-cr2-tFT proteins in tobacco epidermal cells was revealed by quantifying the ratio-metric fluorescent signal of the tFT consisting of mCherry and sfGFP. Values are means ± SEM ($n = 14$). Circles indicate individual data points. Significance was determined by two-sided Student's t test. $^{**}p < 0.01$.

(legend continued on next page)

eight of ten tested cytosolic NatA substrates by masking the recently identified nonAc-X^2/N-degron. Correspondingly, NatA-depleted plants suffer from a global destabilization of proteins and enhanced protein turnover.[24] Also, in human cells, NTA by NatA is generally protective against global protein degradation by masking apoptosis-triggering N-terminal sequence motifs.[25]

In humans, the core NatA subunit, NAA15, serves as the platform for the binding of two additional proteins: NAA50 and Huntingtin yeast partner K (HYPK).[26,27] Biochemical and structural studies of the ternary NatA/E complex consisting of NAA10, NAA50, and NAA15 and the quaternary NatA/E/HYPK complex suggest that HYPK and NAA50 regulate human NatA activity.[28] In contrast to human NAA50, which is the catalytic subunit of NatE and acetylates N termini starting with an iMet followed by S, T, A, V, L, I, F, Y, and K,[29] yeast NAA50 is catalytically dead.[30,31] In yeast, NAA50 serves as a scaffold protein to position the NatA in the proximity of the ribosomal tunnel exit by interaction with the ribosome expansion segment ES7a.[32] Several NatA substrates are less acetylated at their N terminus in yeast mutants lacking NAA50,[29] suggesting that positioning of NatA at the ribosome by NAA50 is critical for NatA activity. The function of NatE/NAA50 in Arabidopsis is still uncertain. Although *At*NAA50 acetylates canonical NatE substrates *in vitro*, no *in vivo* substrate has been identified by global N-acetylome profiling of *naa50* mutants.[33]

HYPK has been evidenced to interact with the NatA complex in humans,[27] *Chaetomium thermophilum*,[34] rice,[35] and Arabidopsis.[36] However, the intrinsically disordered protein was first identified as an interaction partner of the Huntingtin protein[37,38] and was supposed to prevent Huntingtin aggregation by its chaperone-like activity.[39] Later studies showed that HYPK binds to diverse interaction partners related to autophagy and that basal autophagy levels correlated with HYPK steady-state levels in mouse cell lines.[40] In line with these studies, Ghosh and Ranjan propose that HYPK functions as an autophagy receptor for recognizing neddylated proteins during proteotoxic-induced aggrephagy. In this scenario, recognition of the ubiquitin-like protein NEDD8 is mediated by a ubiquitin-associated (UBA) domain located in the C terminus of HYPK.[41]

Remarkably, the interaction of HYPK with NAA15 is conserved in the ternary NatA/HYPK complex of *Chaetomium thermophilum* and humans.[34,42] The HYPK C terminus comprises a UBA domain that forms a three-helix bundle (THB) necessary and sufficient for high-affinity binding to NAA15, while the N-terminal helix α1 locates nearby the NAA10 substrate binding site.[34] The helix α1 of HYPK from *C. thermophilum* and humans is essential for the inhibition of NatA *in vitro*, suggesting that HYPK acts *in vivo* as an inhibitor of NatA activity.[28,34,42] In contrast to these *in vitro* studies, the knockdown of HYPK in human cells does not stimulate NatA activity but prevents N-terminal acetylation of a known NatA substrate.[27] These data suggested that human HYPK may act *in vivo* as a NatA activator. Indeed, mutations in the single copy gene encoding for HYPK in Arabidopsis or rice caused lowered N-terminal acetylation of NatA substrates, and the respective Arabidopsis mutants resembled the phenotype of NatA-depleted Arabidopsis plants.[35,36] These contradicting findings question the role of the helix α1 and the UBA domain of plant HYPK in controlling NatA activity in plants.

In this study, we applied CRISPR-Cas9 genome editing to generate Arabidopsis mutants expressing either a non-functional HYPK due to a premature stop codon at residue 13 (*hypk-cr1*) or an N-terminally deleted HYPK protein truncating the functional helix α1 (*hypk-cr2*). The *hypk-cr1* mutant was complemented with the N-terminal HYPK domain, the C-terminal UBA domain, and the full-length HYPK to understand the contribution of the UBA domain and helix α1 for regulation of NatA activity, NatA-dependent proteostasis, vegetative growth, and response to drought.

RESULTS

The HYPK N terminus is critical for plant growth

The *Arabidopsis thaliana* ecotype Col-0 was transformed with two CRISPR-Cas9 constructs to generate the *hypk-cr1* mutant lacking a functional HYPK protein and the *hypk-cr2* mutant truncating the functional helix α1 of HYPK (Figures 1A and 1B). In *hypk-cr1*, a single base pair insertion at position 31 resulted in a frameshift, which caused a premature stop codon at residue 13 (Figures 1A, S1A, and S1D). In *hypk-cr2*, an in-frame deletion of 224 base pairs of the *HYPK* gene caused the expression of an HYPK protein impaired in helices α1 and α2 due to the deletion of 42 amino acids in the HYPK N terminus (Figures 1A, 1B, and S1B–S1D). The respective mutations in *hypk-cr1* and *hypk-cr2* were verified by genome sequencing (Figures S1A and 1C). The habitus (Figure 1C) and growth rate (Figures 1D and S1G) of *hypk-cr1* were indistinguishable from the previously described *hypk-3* mutants harboring a transfer DNA insertion in exon 2 (Figure 1A). The *hypk-cr2* mutant displayed an intermediate growth rate and habitus, suggesting that the N-terminally truncated HYPK-cr2 protein was partially functional. Genetic complementation revealed that both *hypk-cr1* and *hypk-cr2* mutants can be fully rescued by the full-length *HYPK* protein (Figures S1E and S1F). The HYPK-cr2 protein displayed the same subcellular localization as, and indistinguishable protein stability from, the full-length HYPK when fused to the tandem fluorescent timer (Figures 1E and 1F). We also confirmed the close proximity of HYPK-cr2 protein with NAA15 and NAA10 *in planta* using the split-luciferase system (Figure 1G) that has been previously applied to demonstrate the interaction of core NatA subunits with each other and the full-length HYPK protein.[36] Furthermore, we provided evidence for the direct interaction of the purified core *Ct*NatA with either the *At*HYPK-cr2 protein or the full-length *At*HYPK in a ternary complex by size-exclusion chromatography (Figures 1H and S2). These findings demonstrate that the N-terminally truncated HYPK-cr2 protein is stable and can still

(G) Proof for close proximity between *At*NAA15 and full-length HYPK or truncated HYPK-cr2 in tobacco leaf cells was revealed by reconstitution of luciferase in the split luciferase complementation assay.[45] The previously demonstrated interaction between *At*NAA15 and *At*NAA10 served as a positive control. In the negative control, the catalytic subunit of NatA, NAA10, was replaced with the catalytic subunit of NatB, NAA20.

(H) Physical interactions between purified *Ct*NatA and the full-length HYPK or the truncated HYPK-cr2 were analyzed by analytical size-exclusion chromatography. The shift to a lower elution volume indicates the formation of a ternary complex consisting of *Ct*NatA-*At*HYPK or *Ct*NatA-*At*HYPK-cr2 (Figure S2).

interact with the NatA complex in the cytosol of plants like the full-length HYPK protein.

Loss of HYPK N terminus enhances resilience toward drought stress

Depletion of NatA activity by an RNAi approach causes significant tolerance to water limitation due to closed stomata and a constitutively activated ABA response in the *amiNAA10* and *amiNAA15* mutants.[14] This phenotype is also persistent in the previously identified HYPK transfer DNA insertion lines *hypk-1* and *hypk-3*. Based on these findings, we speculated that HYPK-impaired plants like *hypk-cr2* would also be more resistant to water withdrawal. The *hypk-cr1* was as tolerant to soil drying as the *hypk-3* mutant (Figure 2A), confirming the role of HYPK in stomatal closure and adaptation to water limitation. While significantly less affected in growth than *hypk-cr1*, *hypk-cr2* was substantially more tolerant to water restriction than the wild type of the same developmental stage or the same age (Figure 2A). The stomatal aperture and the water loss of *hypk-cr2* during soil drying were intermediate between wild type and *hypk-cr1* (Figures 2B, 2C, and S3A). Re-watering experiments independently confirmed the substantial drought tolerance of *hypk-cr1* and highlighted the intermediate tolerance to soil drying of *hypk-cr2* when compared to wild type and *hypk-cr1* (Figures S3B and S3C).

Impairment of helix α1 and α2 in HYPK destabilizes the plant proteome

Next, we tested if the N-terminal deletion in the HYPK-cr2 protein variant would also enhance global protein turnover due to the absent masking of N-degrons with acetylation marks.[24,36] We could confirm the increased proteasome activity and higher endogenous poly-ubiquitination rate in the *hypk-3* mutant when compared to wild type and found no statistically significant difference in the activation of the UPS between *hypk-3*, *hypk-cr1*, and *hypk-cr2* (Figures 2D–2F). However, *hypk-cr2* displayed a tendency to be less affected than *hypk-3* and *hypk-cr1*. Also, the translation rate of *hypk-cr2* monitored by incorporation of ^{35}S-isotope-labeled sulfur amino acids or azidohomoalanine into foliar proteins was moderately enhanced when compared to wild type, while the translation was substantially higher in *hypk-3* and *hypk-cr1* (Figures 2G and S4). These findings demonstrate that the N terminus containing the helix α1 of HYPK is critical for proteome stabilization.

The HYPK N terminus is critical for full activation of NatA activity *in planta*

Since proteostasis is affected by decreased NatA activity,[24] we determined the amount of free N termini in *hypk-cr2* and compared it with the quantity of free N termini in the wild type and the total loss of HYPK function mutants *hypk-3* and *hypk-cr1*. The *hypk-cr2* mutant displayed a statistically significant increase in free N termini compared to wild type that was indistinguishable from the increase in *hypk-cr1* and *hypk-3* (Figure 3A). Next, we applied N-terminome profiling to provide direct evidence for decreased NatA activity in *hypk-cr2*. As expected, NTA of proteins starting with the iMet, which are typically NatB, NatC, NatE, or NatF substrates, were not affected in mutants with impaired HYPK function (Figure 3B). In contrast, the bulk of NatA substrates undergoing iMet removal by MetAP were significantly less Nt acetylated in *hypk-cr2* when compared to wild type (Figures 3C and 3D). Endogenous NatA activity was even lower in *hypk-cr1* and *hypk-3*, resulting in a substantial and comparable increase of partially acetylated NatA substrates and less fully acetylated proteins (Figure 3D). This increase of non-acetylated NatA substrates was less pronounced in *hypk-cr2*, suggesting that the presence of the UBA domain in the HYPK-cr2 protein contributes to the maintenance of NatA activity *in planta* (Figure 3D; Table S1). However, full activation of NatA by HYPK required the N-terminal domain of HYPK, including helix α1 and α2. Remarkably, NatA substrates displaying diverse small amino acids at the neo-generated N terminus were less acetylated in *hypk-cr2*, providing direct evidence for the contribution of the HYPK N terminus to efficient acetylation of diverse NatA substrates.

HYPK stabilizes the core NatA specifically in the leaves of plants

In the previously described *hypk-1* and *hypk-3* mutants, transcription of *NAA10* and *NAA15* was not affected.[36] Transcription of *NAA10* and *NAA15* was also unaffected in leaves of *hypk-cr1* and *hypk-cr2* (Figure S5A). However, steady-state protein levels of NAA10 and NAA15 were decreased to 39%–43% of wild-type levels in leaves of *hypk-3* and *hypk-cr1* as determined with specific antisera. In *hypk-cr2*, NAA10 and NAA15 were lowered to 84% and 81% of wild-type levels, respectively (Figures 4A–4D). Such a substantial decrease in NatA core subunits could be responsible for the significantly lowered acetylation of NatA substrates in the *hypk* mutants.

Since we previously did not find any substantial decrease in NAA10 or NAA15 steady-state levels by a mass-spectrometry-based approach in roots of *hypk-1* and *hypk-3*,[36] we also tested NAA10 and NAA15 abundance in roots of the *hypk* mutants. In support of the previous findings, NAA10 and NAA15 were not significantly affected in the roots of all *hypk* mutants, although a tendency for NAA15 to decrease was observed in *hypk-cr1* and *hypk-3* (Figures 4E–4H). To further investigate the regulatory mechanisms of NatA in different organs, we examined the transcript levels and protein amounts of NatA in roots and leaves of hydroponically grown wild type. The protein amounts of NAA10 and NAA15 were significantly lower in roots than in leaves, although the transcript levels of *NAA10*, *NAA15*, and *HYPK* in both organs were comparable, suggesting the presence of unrevealed NatA regulators in roots (Figures S5B and S5C). Next, we profiled the global N-terminomes in roots of the wild type and the *hypk-cr1* mutant and compared them with the N-terminomes detected in leaves of both genotypes. Remarkably, the distribution of NTA yield in the detected proteomes of the roots and the leaves were comparable in the wild type, suggesting that the capacity of the NTA machinery is similar in both organs (Figure 4I). Furthermore, we did not observe significant differences in the NTA level of NatA substrates or proteins starting with an iMet detected in both organs of the wild type (Figure 4J).

As expected, proteins starting with an iMet were not affected in the roots of *hypk-cr1* compared to wild type (Figure 4J). In sharp contrast, the distribution of NTA yield for NatA substrates was significantly lower in the roots of *hypk-cr1* but less affected than in leaves of *hypk-cr1* (Figure 4I; Table S2). These findings suggest

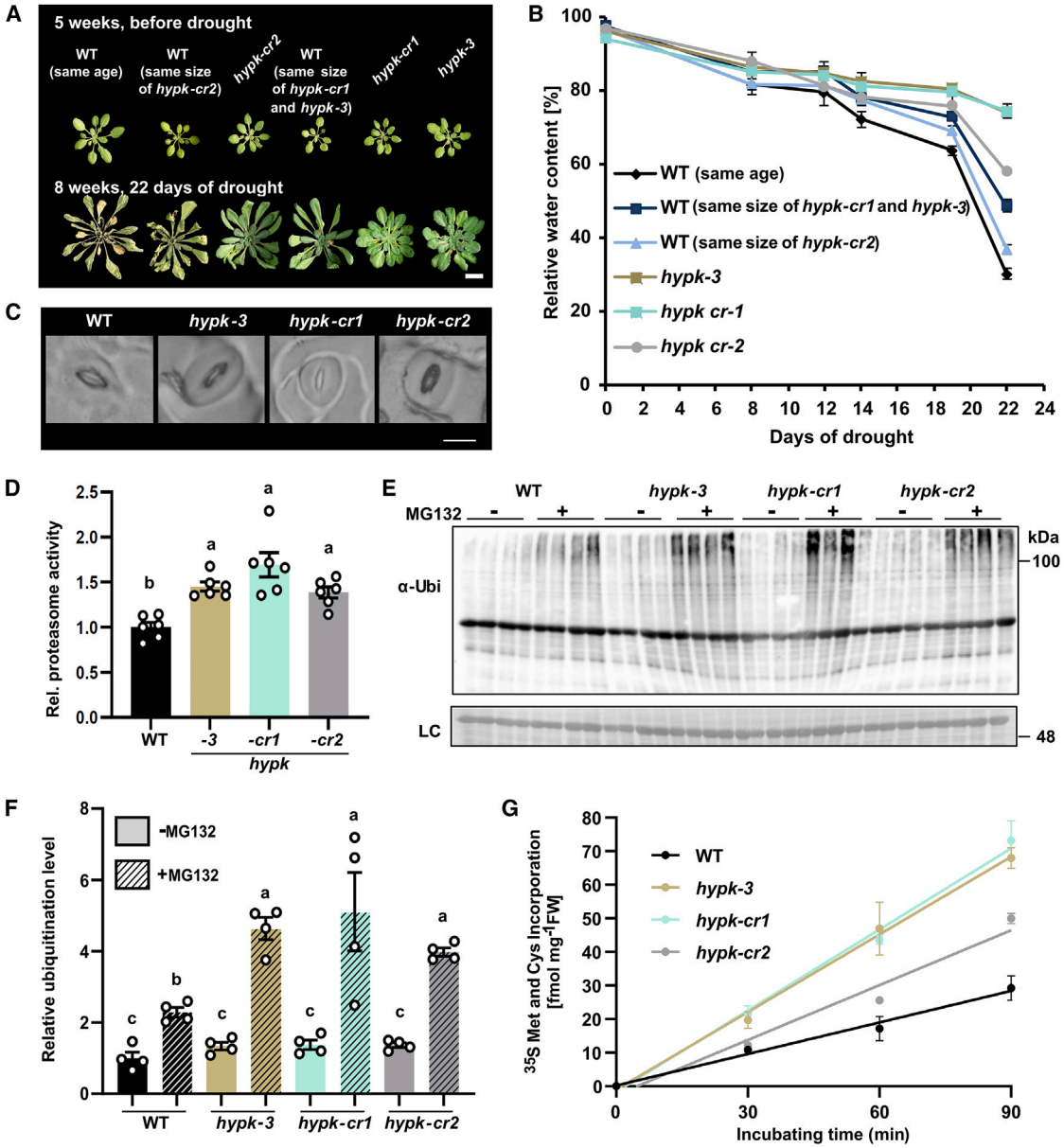

Figure 2. Loss of HYPK N terminus (nHYPK) enhances resilience toward drought stress and leads to accelerated protein turnover

(A) Representative phenotypes of soil-grown WT and *hypk* mutants before (5 weeks old) and after 22 days of water limitation (8 weeks old). We included developmental WT controls for *hypk-cr1* and *hypk-cr2*, displaying precisely the same size as the respective *hypk* mutants at the beginning of the water limitation. The experiment was replicated three times, yielding similar results. Twenty individual plants per genotype were examined for each repetition. Scale bar: 2 cm.

(B) Relative water content of the WT controls and the *hypk* mutants during water restriction. The *hypk-cr1* and *hypk-cr2* plants were more resistant to water restriction than WT plants of the same age or the same size. Data are shown as means ± SEM (n = 3).

(C) Focus on representative stomata in epidermal imprints of leaves from well-watered 6-week-old plants grown on soil. Scale bar: 10 μM.

(D) Quantitation of proteasome activity in leaves of 6-week-old soil-grown WT and *hypk* mutants. Data are shown as means ± SEM (n = 6). Circles indicate individual data points. Different letters indicate individual groups identified by pairwise multiple comparisons with a one-way ANOVA followed by a Tukey's test ($p < 0.05$).

(E and F) Detection (E) and quantitation (F) of global mono- and poly-ubiquitination levels with the specific antiserum ubiquitin FK2 (BML-PW8810, Enzo Life Sciences) in the WT and *hypk* mutants in the presence (dashed bars) or absence (filled bars) of the proteasome inhibitor MG132. Rubisco served as an internal loading control (LC). Data are shown as means ± SEM (n = 4). Circles indicate individual data points. Different letters indicate individual groups identified by pairwise multiple comparisons with a one-way ANOVA followed by a Tukey's test ($p < 0.05$).

(G) Translation rate in the WT and *hypk* mutants monitored by incorporation of ^{35}S-isotope-labeled sulfur amino acids into foliar proteins of 6-week-old soil-grown plants (n = 3).

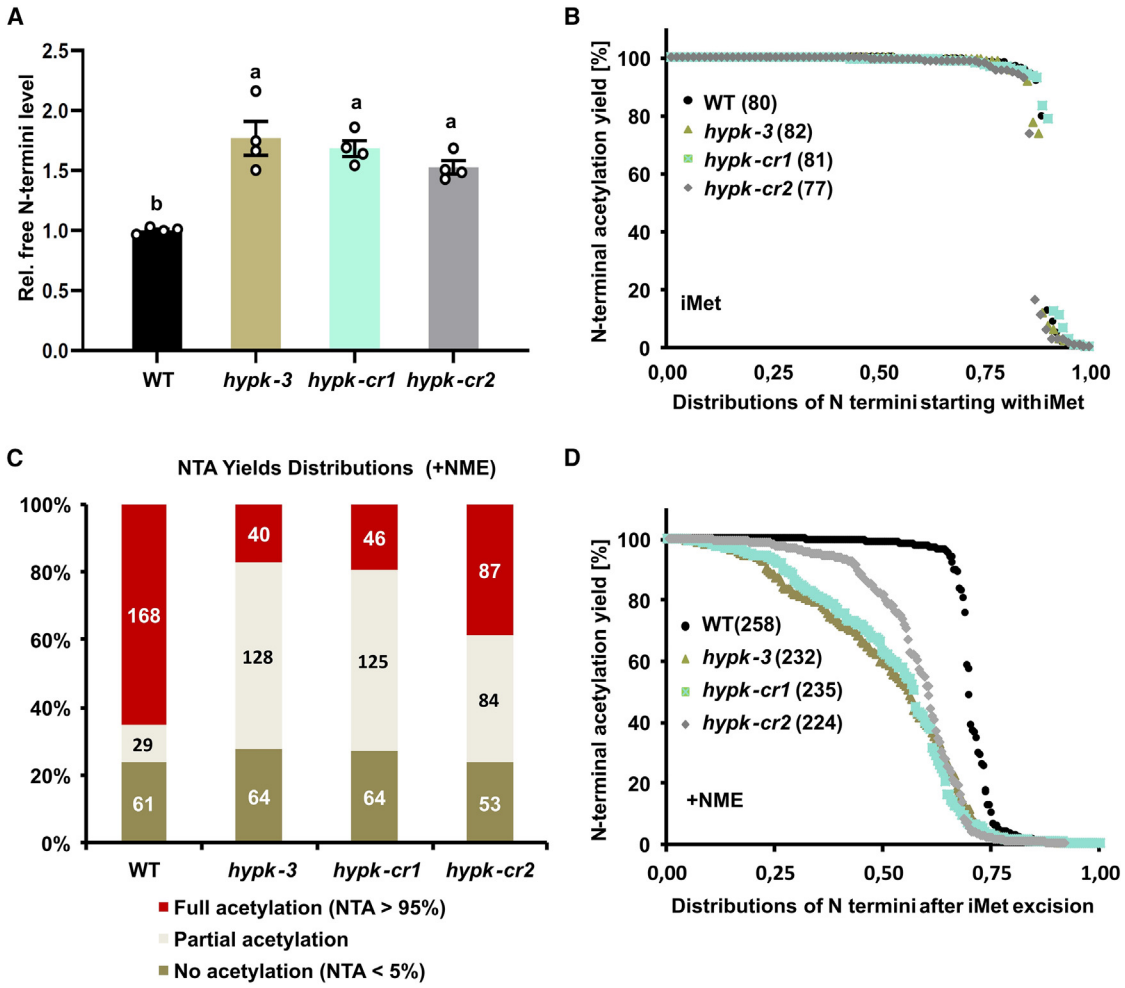

Figure 3. HYPK specifically regulates NatA-mediated N-terminal acetylation, and both the N and C termini of HYPK contribute to the regulation of NatA activity

(A) Relative quantification of free N-terminal level in the soluble foliar protein fraction of soil-grown 6-week-old WT and *hypk* mutants as determined by staining with the fluorescent dye (NBD-Cl). Data are shown as means ± SEM. Circles indicate individual data points. Different letters indicate individual groups identified by pairwise multiple comparisons with a one-way ANOVA followed by a Tukey's test ($p < 0.05$, $n = 4$).

(B) Distribution for N-terminal acetylation yields of peptides starting with the iMet (predicted substrates of NatB, NatC, and NatE) in leaves of WT and *hypk* mutants as determined by the SILProNAQ.[46] Numbers in brackets display the quantity of detected N termini.

(C) Comparison of fully (red), partially (gray), and non-acetylated (olive) protein N termini that were subject to iMet excision (+NME, predicted NatA substrates) in leaves of WT and the *hypk* mutants. Numbers in the bars represent the quantity of characterized N termini in this fraction.

(D) Distribution for N-terminal acetylation yields of predicted NatA substrates in leaves of WT and *hypk* mutants as determined by the SILProNAQ mass spectrometry approach. Numbers in brackets display the quantity of detected N termini.

that the significant destabilization of both core NatA subunits contributed to the lowered endogenous NatA activity in leaves and that HYPK facilitates acetylation of NatA substrates in roots predominantly without affecting the stability of the core NatA.

The triple-helix bundle formed by the UBA domain is essential for HYPK function

To dissect the function of the UBA domain and the N terminus of HYPK in the *in vivo* stabilization of core NatA, we complemented the *hypk-cr1* mutant with DNA constructs, allowing the expression of the full-length HYPK$^{1–115}$, the N terminus of HYPK$^{1–63}$, or the C terminus including the UBA domain of HYPK$^{63–115}$ under the control of the strong 35S promotor (Figure 5A). As expected, expression of the full-length HYPK fully rescued the retarded growth phenotype of *hypk-cr1* (Figure 5B, S6A, and S6B) by restoring NatA activity (Figures 5C, S6C, and S6D; Table S3) due to stabilizing NAA10 (Figure 5D) and NAA15 (Figure 5E). Expression of the N terminus of HYPK$^{1–63}$ in *hypk-cr1* did not rescue growth-phenotype, NatA-mediated NTA by stabilizing the core NatA subunits (Figures 5B–5E and S6; Table S3), strongly suggesting that interaction of HYPK via the C-terminal UBA domain is critical for the NatA-facilitating function of the HYPK N terminus. In line with this idea, the expression of HYPK$^{63–115}$ partially rescued the growth phenotype of *hypk-cr1* by restoring the NTA yield and stabilizing NatA

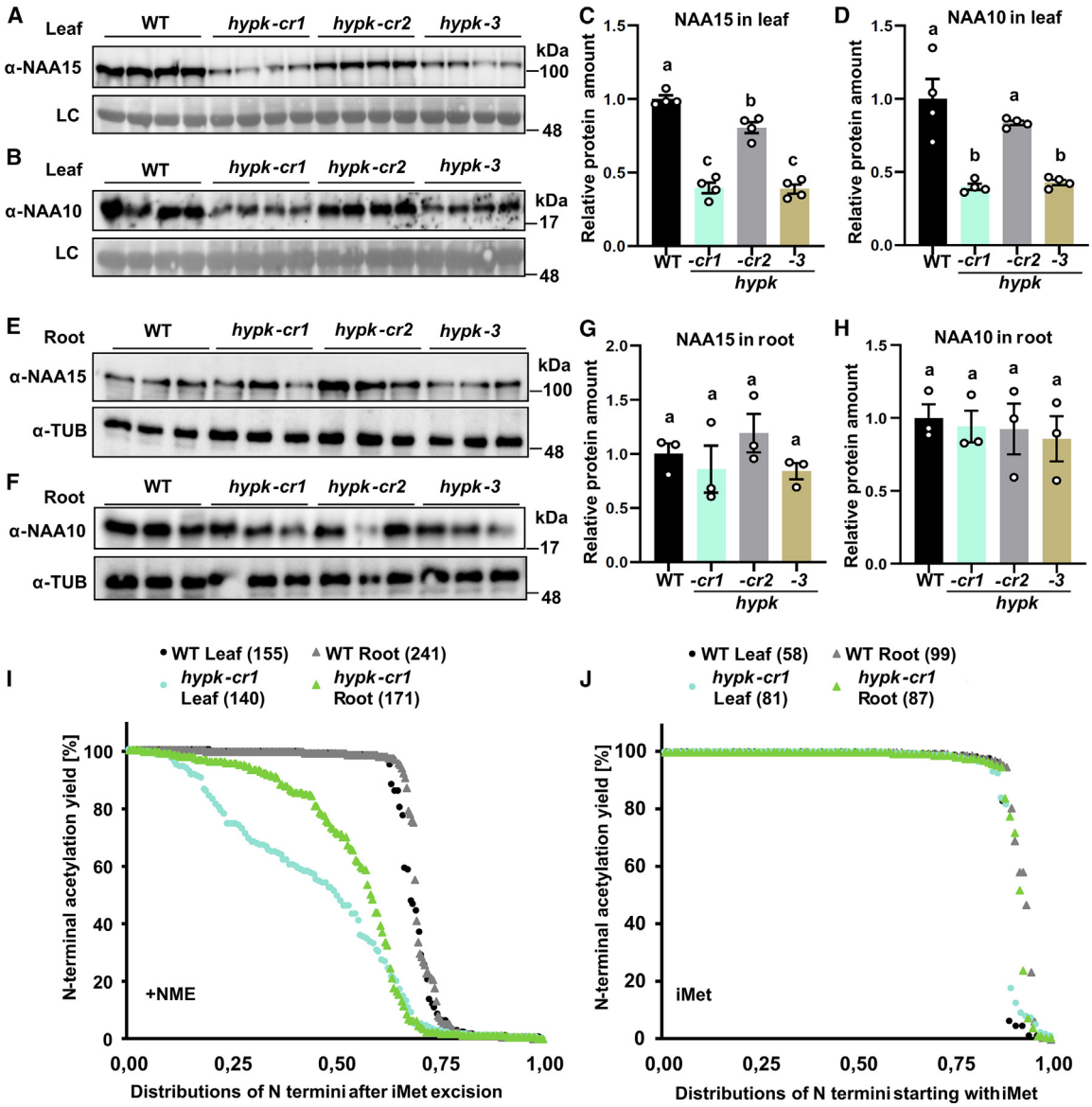

Figure 4. HYPK regulates the protein amount of NatA in a tissue-specific manner

(A and B) Immunological detection of NAA15 (A) and NAA10 (B) protein levels in leaves of WT and *hypk* mutants with specific antisera against NAA15 and NAA10.

(C and D) Quantification of NAA15 (C) and NAA10 (D) abundance according to immunological detection shown in (A) and (B). Data are shown as means ± SEM. Circles indicate individual data points. Different letters indicate individual groups identified by pairwise multiple comparisons with a one-way ANOVA followed by a Tukey's test ($p < 0.05$, $n = 4$).

(E and F) Immunological detection of NAA15 (E) and NAA10 (F) protein levels in roots of hydroponically grown WT and *hypk* mutants with specific antisera against NAA15 and NAA10.

(G and H) Quantification of NAA15 (G) and NAA10 (H) abundance in roots according to immunological detection shown in (E) and (F). Data are shown as means ± SEM. Circles indicate individual data points. Different letters indicate individual groups identified by pairwise multiple comparisons with a one-way ANOVA followed by a Tukey's test ($p < 0.05$, $n = 3$).

(I and J) Distribution for N-terminal acetylation yields of predicted NatA substrates (I) and N termini starting with the iMet (J) in leaves and roots of hydroponically grown WT and *hypk-cr1* as determined by the SILProNAQ mass spectrometry approach.[46] The number in brackets displays the quantity of detected N termini.

subunits to a *hypk-cr2*-like intermediate level (Figures 5B–5E and S6; Table S3). Remarkably, the phenotype of transgenic plants complemented with the UBA domain encoded in the C terminus of HYPK was indistinguishable from *hypk-cr2* (Figures 5B and S6B).

HYPK stabilizes NAA15 in leaves

In humans, HYPK has an intrinsic chaperone activity and is connected to the autophagy of aggregated proteins.[41,47] Based on our results, we suggested that the primary function of plant HYPK is to facilitate NatA activity. To test this hypothesis, we

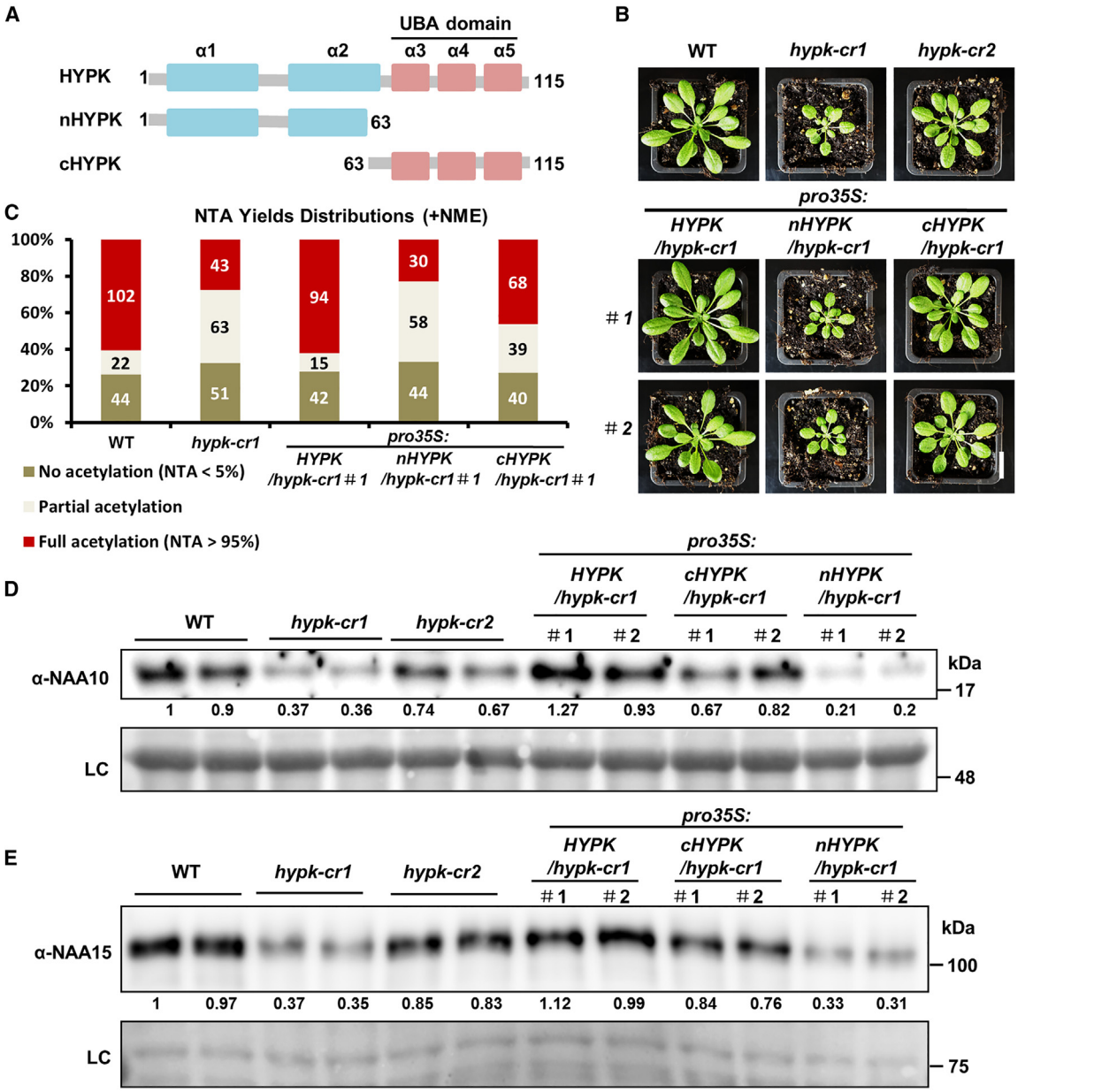

Figure 5. The C terminus of HYPK is required for proper NatA activity and plant growth

(A) Schematic representation of secondary structure elements in the full-length HYPK$^{1–115}$ and the truncated protein variants nHYPK (HYPK$^{1–63}$) and cHYPK (HYPK$^{63–115}$) used for complementation of *hypk-cr1* under control of the 35S CaMV promoter (*pro35S*).

(B) Representative phenotype of 5-week-old soil-grown WT, *hypk-cr1*, *hypk-cr2*, and two independent *hypk-cr1* lines complemented with either the full-length HYPK (*pro35S*:*HYPK*) or the truncated HYPK variant nHYPK (*pro35S*:*nHYPK*) or cHYPK (*pro35S*:*cHYPK*).

(C) Comparison of fully (red), partially (gray), and non-acetylated (olive) protein N termini that were subject to iMet excision (+NME, predicted NatA substrates) in leaves of WT, *hypk-cr1*, and *hypk-cr1* complemented with the full-length HYPK, the nHYPK, or the UBA domain of HYPK (cHYPK). Numbers in the bars represent the quantity of characterized N termini in this fraction.

(D and E) Immunological detection of NAA10 (D) and NAA15 (E) in leaves of WT, *hypk-cr1*, *hypk-cr2*, and complemented *hypk-cr1* lines with specific antisera (α-NAA10 and α-NAA15). Amido black staining of proteins transferred to the PVDF membrane served as LC. Numbers below the immunological detection indicate the abundance of the respective protein species relative to the signal in the WT replicate 1 after internal normalization to the LC.

overexpressed the catalytic NatA subunit NAA10 in *hypk-cr1* and tested for the complementation of the phenotype. We identified ten *pro35S*:*NAA10*/*hypk-cr1* lines that were transformed, with the DNA construct allowing the expression of NAA10 under the control of the 35S-cauliflower mosaic virus promotor. These lines were phenotypically fully complemented under the here-applied growth conditions (Figures 6A and S7). We selected lines 1 and 2 as representatives for further analyses. Ectopic

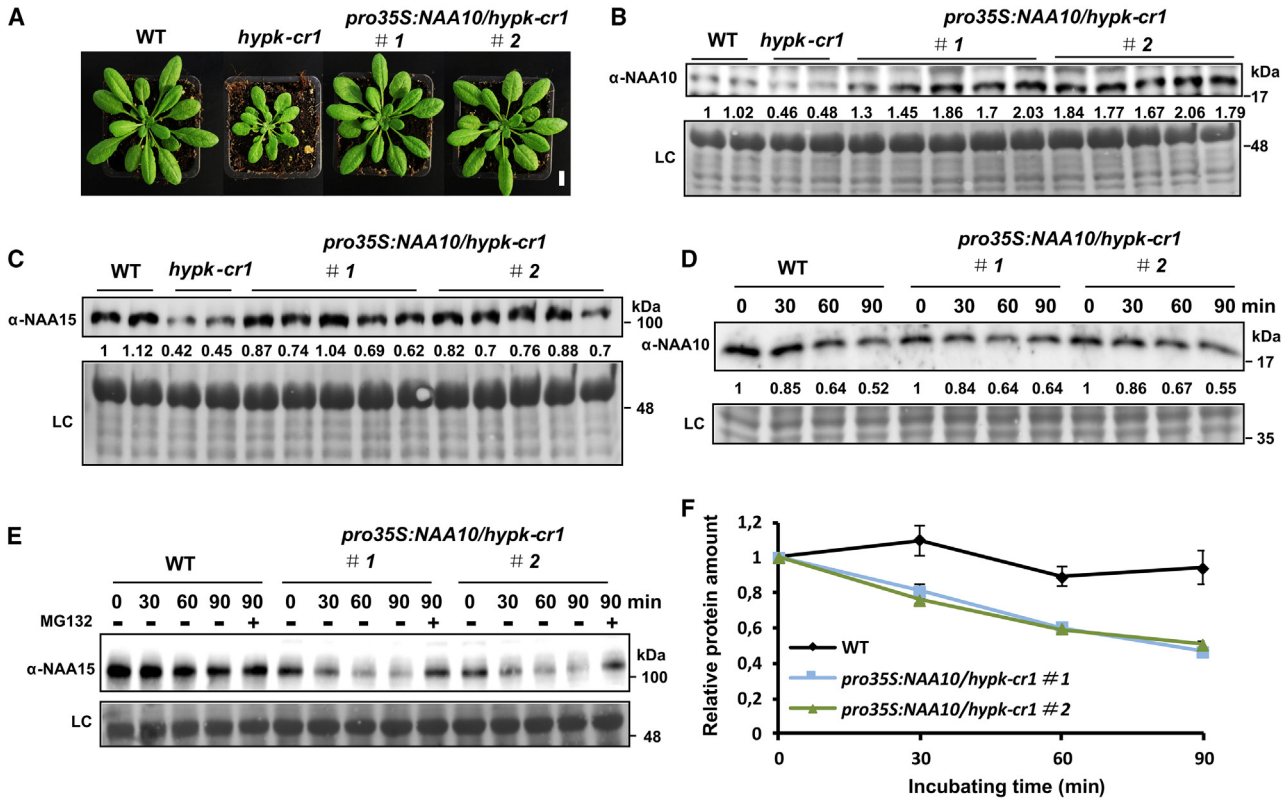

Figure 6. Ectopic expression of NAA10 in *hypk-cr1* rescues the *hypk-cr1* phenotype and stabilizes NAA15

(A) Representative image of 6-week-old soil-grown WT, *hypk-cr1*, and two *hypk-cr1* lines independently complemented with the *AtNAA10* gene under the control of the *35S* CAMV promoter (*pro35S:NAA10*).

(B and C) Immunological detection of NAA10 (B) and NAA15 (C) in leaves of WT, *hypk-cr1*, and complemented *hypk-cr1* lines with specific antisera (α-NAA10 and α-NAA15). Amido black staining of proteins transferred to the PVDF membrane served as LC. Numbers below the immunological detection indicate the abundance of the respective protein species relative to the signal in the WT replicate 1 after internal normalization to the LC.

(D) Degradation rate of NAA10 in the leaves of WT and the complemented *hypk-cr1* lines by a cell-free degradation assay.

(E and F) Detection (E) and quantification of NAA15 (F) degradation rate in the leaves of WT and the complemented *hypk-cr1* lines by a cell-free degradation assay. Degradation rate is based on immunological detection of NAA10 (D) and NAA15 (E) with specific antisera (α-NAA10 and α-NAA15) at indicated time points. Amido black staining of proteins transferred to the PVDF membrane served as LC. Numbers below the immunological detection represent the abundance of the individual protein species relative to the signal in the WT at time point zero. Absence of HYPK in leaves of the *pro35S:NAA10/hypk-cr1* complemented lines results in substantially faster degradation of NAA15 when compared to WT, while the NAA10 degradation rate was unaffected by loss of HYKP. In (E), the proteasome activity was inhibited in controls with 50 μM MG132 (+MG132).

expression of *At*NAA10 in *hypk-cr1* increased the steady-state level of NAA10 from the 0.5-fold wild-type level in *hypk-cr1* to up to 2-fold of the wild-type level in both transgenic lines (Figure 6B). The accumulation of NAA10 resulted in a partial rescue of NAA15 steady-state levels in both transgenic lines (Figure 6C). These results imply that the dominant function of plant HYPK is to facilitate the activity of NatA and that this is partially achieved by stabilizing the NatA core subunits in leaves. Accumulation of both core NatA subunits in the *pro35S:NAA10/hypk-cr1* lines enabled us to test their degradation rate in the *hypk-cr1* background with a cell-free degradation approach. While the degradation rate of NAA10 was not affected in *hypk-cr1* (Figure 6D), the degradation of NAA15 was significantly faster in both *pro35S:NAA10/hypk-cr1* transgenic lines (Figures 6E, 6F, and S8). The latter finding strongly suggests that NAA15 is unstable in leaves of *hypk-cr1*, which might be causative for lower NAA15 steady-state levels in leaves of *hypk-cr1*. Since the down-regulation of NAA15 in *amiNAA15* lines also decreases the NAA10 steady-state level in leaves,[14] NAA15 destabilization in *hypk-cr1* might also impair the accumulation of the catalytic NAA10 subunit.

HYPK promotes NatA activity not only by protecting NatA from degradation

NatA activity is significantly decreased in roots of *hypk-cr1*, although accumulation of both NatA core subunits is almost unaffected (Figure 4). Thus, we wanted to test if HYPK has, on top of the stabilizing impact, an additional NatA-facilitating function in leaves. For this purpose, we crossed *hypk-cr1* with *muse6*-1 (Figures S9A and S9B), which suffers from lower NAA15 levels due to a stable single-point mutation affecting the splicing of the *NAA15* mRNA.[15] We expected a worsening phenotype in the *muse6-1 hypk-cr1* double mutant accompanied by further destabilization of NAA15 if the only function of HYPK is to

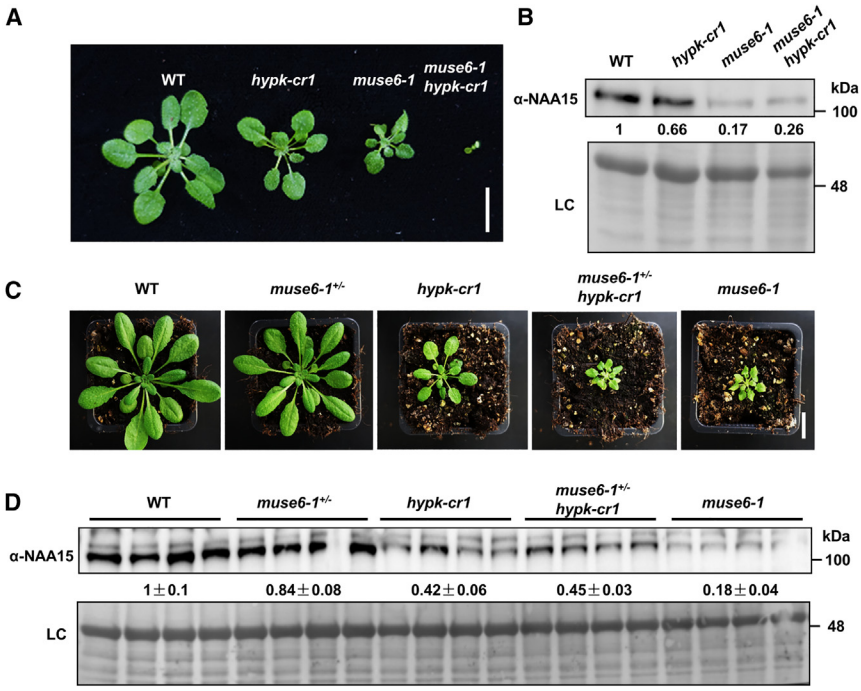

Figure 7. HYPK additionally regulates NatA activity in a stability-independent manner and is essential for the proper function of NAA15

(A) Phenotype of 4-week-old soil-grown WT, *hypk-cr1*, the NAA15-depleted mutant *muse6-1*, and the *muse6-1 hypk-cr1* double mutant.

(B) Immunological detection of NAA15 protein amount in leaves of WT, *hypk-cr1*, *muse6-1*, and the *muse6-1 hypk-cr1* double mutant with a specific antiserum (α-NAA15). Amido black staining of proteins transferred to the PVDF membrane served as LC. Numbers below the immunological detection indicate the abundance of the respective protein species relative to the signal in the WT after internal normalization to the LC. Despite the substantial growth deterioration of the *muse6-1 hypk-cr1* double mutant when compared to *muse6-1*, NAA15 steady-state levels were indistinguishable in both lines.

(C and D) Phenotype (C) and NAA15 abundance (D) in leaves of 6-week-old soil-grown WT, heterozygous *muse6-1*$^{+/-}$, *hypk-cr1*, the *muse6-1*$^{+/-}$ *hypk-cr1* (heterozygous for the *muse6* allele), and the homozygous *muse6-1* plants. Introduction of the heterozygous *muse6* allele in the *hypk-cr1* background worsened the phenotype of the *muse6-1*$^{+/-}$ *hypk-cr1* double mutant plants when compared to *hypk-cr1* (C) without further depletion of NAA15 steady-state levels (D). Although the *muse6-1*$^{+/-}$ *hypk-cr1* double mutant plants were indistinguishable from homozygous *muse6-1*, NAA15 levels were significantly higher than in *muse6-1*, demonstrating that HYPK can facilitate *in vivo* NatA activity on top of its stabilizing impact on NAA15. Numbers represent the means ± SEM (n = 4).

stabilize NAA15. If HYPK has an additional NatA-facilitating function, we expect a worsening phenotype without further destabilizing the already low levels of NAA15 in the double mutant. The homozygous *muse6-1 hypk-cr1* double mutants displayed an extremely dwarf phenotype and could not survive past the 6-leaf stage under applied conditions (Figures 7A, S9C, and S9D). Remarkably, NAA15 steady-state levels in the *muse6-1 hypk-cr1* double mutant were indistinguishable from the parental line *muse6-1* (Figure 7B). Crosses of homozygous *hypk-cr1* with heterozygous *muse6-1*$^{+/-}$ displayed the same NAA15 steady-state level as *hypk-cr1* but grew worse than *hypk-cr1* (Figures 7C, 7D, S9E, and S9F). The *muse6-1*$^{+/-}$ *hypk-cr1* plants were indistinguishable from the homozygous *muse6-1*, suffering from a decrease to 18% of NAA15 wild type level, although *muse6-1*$^{+/-}$ *hypk-cr1* maintained 45% of the NAA15 wild-type level. Taken together, these findings demonstrate that HYPK not only stabilizes NAA15 in leaves but also promotes foliar NatA activity by an independent mechanism.

DISCUSSION

We previously showed that the NatA complex promotes the stability of the Arabidopsis proteome by imprinting approximately 50% of cytosolic proteins with acetylation marks.[14,24] This imprinting of the N terminus occurs co-translationally when 40 amino acids of the nascent chain emerge from the ribosomal tunnel exit[48] and requires co-translational removal of the iMet by MetAP. Both processes must be dynamically controlled since translation speed is about 5–9 amino acids per second in eukaryotes.[49] Furthermore, diverse ribosome-associated factors compete for scanning of the nascent chain to determine the correct subcellular localization of the nascent chain and assist in folding the newly synthesized cytosolic proteins. Consequently, positioning NatA in close proximity to the ribosomal tunnel exit at the right time is crucial for successfully masking N-degrons in proteins.

In yeast, this positioning of the core NatA complex is achieved by the interaction of the ribosome expansion segment 27a with NAA15 and of ES7a with the enzymatically dead yeast NAA50 protein.[32] In humans and Arabidopsis, NAA50 is enzymatically active, and its knockout does not impair plant NatA activity as determined by N-terminome profiling.[33,49] Instead, HYPK is critical for *in vivo* NatA activity in Arabidopsis, rice, and humans,[27,35,36] suggesting that HYPK supports the positioning of the core NatA at the ribosome for acetylation of NatA substrates in higher eukaryotes. Here, we provide direct evidence that the absence of HYPK in Arabidopsis is not lethal but strongly impairs *in vivo* NatA activity. The viability of *hypk-cr1* demonstrates that HYPK is not part of the essential core NatA complex, which agrees with the biochemical analysis of the core NatA and NAA10 activity *in vitro* and the loss of HYPK in yeast.[50,51] In leaves, HYPK absence resulted in substantial destabilization of NAA15, also causing depletion of NAA10. Consequently, HYPK loss-of-function mutants resemble the phenotype of NatA-depleted mutants. Destabilization of core NatA subunits in leaves was significantly reverted by ectopic expression of the THB formed by the UBA domain of HYPK. If the UBA domain of HYPK shields an intrinsic degron exposed in free NAA15 and/or if the UBA domain of HYPK promotes the association of the core NatA with ribosomes to stabilize the core NatA remains elusive, but it is tempting to speculate.

HYPK-triggered stabilization of the core NatA subunits was only marginal in roots, probably due to differences in the UPS of both organs.[52,53] However, *hypk-cr1* roots also suffered from lowered NTA of NatA substrates, suggesting that *At*HYPK possesses an additional NatA activity-promoting function. Also, in rice, HYPK does not stabilize core NatA subunits but is critical for the full activation of NatA.[35] The N termini of *Hs*HYPK and *Ct*HYPK control peptide access into the active site of NAA10 *in vitro*.[34,42] Prediction of the *At*HYPK structure with AlphaFold suggests the conservation of helix α1, which binds close to the active site of *Ct*NAA10 in the ternary *Ct*NatA/*Ct*HYPK complex.[34] Truncation of the predicted helix α1 and α2 in the *hypk-cr2* mutant caused a significant accumulation of non-acetylated NatA substrates. It resembled the phenotype of NatA activity-depleted plants, albeit the THB of HYPK was unaffected, and the HYPK-cr2 displayed the same subcellular localization and stability as the full-length HYPK protein in plants. Overexpression of $HYPK^{1-63}$, comprising helix α1 and α2 but not the UBA domain forming the THB, failed to rescue the loss of HYPK or restore wild-type-like NatA activity. Based on these findings, we hypothesize that helix α1 of HYPK promotes the targeting of the nascent NatA substrate into the active site of NAA10 when HYPK is correctly positioned by the physical interaction of the UBA domain with NAA15 at the ribosome nascent chain complex.

The UBA domain of the human HYPK has been recently suggested to act as an autophagy receptor recognizing neddylated cargo during the clearance of protein aggregates.[41] Although many components of the aggrephagy pathways are conserved between plants and humans,[54] we could entirely rescue the phenotype of *hypk-cr1* by restoring NatA activity, questioning a significant contribution of plant HYPK as a receptor for neddylated proteins under non-stressed conditions.

NatA activity is controlled by the stress-related plant hormone abscisic acid and is critical for responding to diverse protein-harming stresses like heat stress, drought, pathogen attack, and salinity,[14,15,55] strongly suggesting that masking of nonAc/N-degron contributes substantially to cellular surveillance by enabling dynamic plasticity of the proteome upon environmental stimuli. Since *hypk-cr2* is also impaired in masking nonAc/N-degrons and the response to water limitation, we suggest that these physiological responses require tight coordination of the emerging N terminus between ribosome-associated factors like MetAP and NatA. In this context, it is noteworthy that the NatB and NatE complex, targeting proteins starting with an iMet, are also critical for diverse stress responses in plants.[16,17,33] These findings corroborate the hypothesis that the eukaryotic ribosome is a hub for protein quality control mechanisms,[56] allowing organisms to adjust the proteome inventory dynamically upon external or internal cues.

Limitations of the study

Our study uncovers that HYPK stabilizes the core NatA complex in the leaves of *Arabidopsis thaliana* by preventing NAA15 from being destroyed by the UPS. However, we have not yet identified the ubiquitin E3-ligase targeting NAA15 for degradation and thus could not address the organ-specific differences in HYPK-mediated NatA stabilization. Although we add significant information on the functional relevance of helix α1 and α2 in the HYPK N terminus and the C-terminal UBA domain forming the THB, further studies are required to unravel how the helix α1 supports NatA activity at the ribosome. A potential avenue to address this delicate question is the expression of a tagged HYPK version allowing for co-purifying ribosome-associated HYPK/NatA complexes, which can be subjected to cryogenic electron microscopy studies.

STAR★METHODS

Detailed methods are provided in the online version of this paper and include the following:

- KEY RESOURCES TABLE
- RESOURCE AVAILABILITY
  - Lead contact
  - Materials availability
  - Data and code availability
- EXPERIMENTAL MODEL AND STUDY PARTICIPANT DETAILS
  - Plant materials
  - Seed germination assays and growth conditions
- METHOD DETAILS
  - Constructs for genetic transformation
  - Stable transformation of *A. thaliana* and selection of transgenic plants
  - Extraction of genomic DNA and genotyping
  - RNA extraction, cDNA synthesis and real-time PCR
  - Protein extraction from Arabidopsis leaf and root tissues
  - SDS-PAGE and immunological detection
  - Subcellular localization and determination of protein stability
  - Firefly luciferase complementation imaging assay
  - Analytical size exclusion chromatography
  - Quantification of the drought stress response
  - Determination of stomatal aperture
  - Determination of proteasome activity
  - Inhibition of proteasome activity with MG132
  - Quantification of global translation by isotope labeling
  - Detection of newly translated proteins by L-azidohomoalanine labeling
  - Determination of free N terminus levels
  - Quantification of the N-terminal acetylome
  - Cell-free protein degradation assay
  - Prediction of protein structure
- QUANTIFICATION AND STATISTICAL ANALYSIS
  - Accession numbers

SUPPLEMENTAL INFORMATION

Supplemental information can be found online at https://doi.org/10.1016/j.celrep.2024.113768.

ACKNOWLEDGMENTS

The authors would like to thank Olga Keberlein and Fabian Bradic for technical support. This work was supported by the Deutsche Forschungsgemeinschaft (DFG, German Research Foundation) with the project-IDs 496871662 (research grant WI 3560/7-1 and He 1848/20-1) to M.W. and R.H. and the

Leibniz Programme (SI586/6-1) to I.S. KatNat (ERA-NET, ANR-17-CAPS-0001-01) and CanMore (France-Germany PRCI, ANR-20 CE92-0040) grants funded by the French National Research Agency (ANR) were awarded to C.G. to support J.-B.B. This work has benefited from the facilities and expertise of the I2BC proteomic platform (Proteomic-Gif, SICaPS) supported by IBiSA, Ile de France Region, Plan Cancer, CNRS, and Paris-Saclay University and from ProteoCure COST (European Cooperation in Science and Technology) action CA20113. The proteomic experiments were partially supported by Agence Nationale de la Recherche under projects ProFI (Proteomics French Infrastructure, ANR-10-INBS-08). This work has benefited from the support from a French State grant (Saclay Plant Sciences, ANR-17-EUR-0007, EUR SPS-GSR) under a France 2030 program (ANR-11-IDEX-0003).

AUTHOR CONTRIBUTIONS

X.G. generated the *hypk-cr1* and *hypk-cr2* mutants under supervision of Y.W. S.G. and M.P. contributed to the drought stress experiments. J.W. and I.S. performed the analytical size-exclusion chromatography and contributed to structural modeling and data interpretation. J.-B.B., T.M., and C.G. performed the N-terminome mass spectrometry analysis in different plant organs. All other experiments were performed by X.G. R.H., M.W., and X.G. designed the study, and X.G. and M.W. wrote the manuscript. C.G., T.M., I.S., R.H., and M.W. acquired funding. All authors reviewed the manuscript.

DECLARATION OF INTERESTS

The authors declare no competing interests.

Received: July 28, 2023
Revised: December 12, 2023
Accepted: January 25, 2024

REFERENCES

1. Linster, E., and Wirtz, M. (2018). N-terminal acetylation: an essential protein modification emerges as an important regulator of stress responses. J. Exp. Bot. *69*, 4555–4568. https://doi.org/10.1093/jxb/ery241.
2. Aksnes, H., Ree, R., and Arnesen, T. (2019). Co-translational, Post-translational, and Non-catalytic Roles of N-Terminal Acetyltransferases. Mol. Cell *73*, 1097–1114. https://doi.org/10.1016/j.molcel.2019.02.007.
3. Drazic, A., Myklebust, L.M., Ree, R., and Arnesen, T. (2016). The world of protein acetylation. Biochim. Biophys. Acta *1864*, 1372–1401. https://doi.org/10.1016/j.bbapap.2016.06.007.
4. Linster, E., Layer, D., Bienvenut, W.V., Dinh, T.V., Weyer, F.A., Leemhuis, W., Brünje, A., Hoffrichter, M., Miklankova, P., Kopp, J., et al. (2020). The Arabidopsis Nα-acetyltransferase NAA60 locates to the plasma membrane and is vital for the high salt stress response. New Phytol. *228*, 554–569. https://doi.org/10.1111/nph.16747.
5. Giglione, C., and Meinnel, T. (2021). Evolution-Driven Versatility of N Terminal Acetylation in Photoautotrophs. Trends Plant Sci. *26*, 375–391. https://doi.org/10.1016/j.tplants.2020.11.012.
6. Ree, R., Varland, S., and Arnesen, T. (2018). Spotlight on protein N-terminal acetylation. Exp. Mol. Med. *50*, 1–13. https://doi.org/10.1038/s12276-018-0116-z.
7. Aksnes, H., McTiernan, N., and Arnesen, T. (2023). NATs at a glance. J. Cell Sci. *136*, jcs260766. https://doi.org/10.1242/jcs.260766.
8. Pożoga, M., Armbruster, L., and Wirtz, M. (2022). From Nucleus to Membrane: A Subcellular Map of the N-Acetylation Machinery in Plants. Int. J. Mol. Sci. *23*, 14492. https://doi.org/10.3390/ijms232214492.
9. Bienvenut, W.V., Brünje, A., Boyer, J.-B., Mühlenbeck, J.S., Bernal, G., Lassowskat, I., Dian, C., Linster, E., Dinh, T.V., Koskela, M.M., et al. (2020). Dual lysine and N-terminal acetyltransferases reveal the complexity underpinning protein acetylation. Mol. Syst. Biol. *16*, e9464. https://doi.org/10.15252/msb.20209464.
10. Dinh, T.V., Bienvenut, W.V., Linster, E., Feldman-Salit, A., Jung, V.A., Meinnel, T., Hell, R., Giglione, C., and Wirtz, M. (2015). Molecular identification and functional characterization of the first N^a-acetyltransferase in plastids by global acetylome profiling. Proteomics *15*, 2426–2435. https://doi.org/10.1002/pmic.201500025.
11. Koskela, M.M., Brünje, A., Ivanauskaite, A., Grabsztunowicz, M., Lassowskat, I., Neumann, U., Dinh, T.V., Sindlinger, J., Schwarzer, D., Wirtz, M., et al. (2018). Chloroplast Acetyltransferase NSI Is Required for State Transitions in Arabidopsis thaliana. Plant Cell *30*, 1695–1709. https://doi.org/10.1105/tpc.18.00155.
12. Asensio, T., Dian, C., Boyer, J.-B., Rivière, F., Meinnel, T., and Giglione, C. (2022). A Continuous Assay Set to Screen and Characterize Novel Protein N-Acetyltransferases Unveils Rice General Control Non-repressible 5-Related N-Acetyltransferase2 Activity. Front. Plant Sci. *13*, 832144. https://doi.org/10.3389/fpls.2022.832144.
13. Meinnel, T., and Giglione, C. (2022). Amino terminal modifications, the associated processing machinery, and their evolution in plastid-containing organisms. J. Exp. Bot. *73*, 6013–6033. https://doi.org/10.1093/jxb/erac290.
14. Linster, E., Stephan, I., Bienvenut, W.V., Maple-Grødem, J., Myklebust, L.M., Huber, M., Reichelt, M., Sticht, C., Møller, S.G., Meinnel, T., et al. (2015). Downregulation of N-terminal acetylation triggers ABA-mediated drought responses in Arabidopsis. Nat. Commun. *6*, 7640. https://doi.org/10.1038/ncomms8640.
15. Xu, F., Huang, Y., Li, L., Gannon, P., Linster, E., Huber, M., Kapos, P., Bienvenut, W., Polevoda, B., Meinnel, T., et al. (2015). Two N-terminal acetyltransferases antagonistically regulate the stability of a nod-like receptor in Arabidopsis. Plant Cell *27*, 1547–1562. https://doi.org/10.1105/tpc.15.00173.
16. Huber, M., Armbruster, L., Etherington, R.D., De La Torre, C., Hawkesford, M.J., Sticht, C., Gibbs, D.J., Hell, R., and Wirtz, M. (2021). Disruption of the Nα-Acetyltransferase NatB Causes Sensitivity to Reductive Stress in Arabidopsis thaliana. Front. Plant Sci. *12*, 799954.
17. Huber, M., Bienvenut, W.V., Linster, E., Stephan, I., Armbruster, L., Sticht, C., Layer, D., Lapouge, K., Meinnel, T., Sinning, I., et al. (2020). NatB-Mediated N-Terminal Acetylation Affects Growth and Biotic Stress Responses. Plant Physiol. *182*, 792–806. https://doi.org/10.1104/pp.19.00792.
18. Vierstra, R.D. (2009). The ubiquitin-26S proteasome system at the nexus of plant biology. Nat. Rev. Mol. Cell Biol. *10*, 385–397. https://doi.org/10.1038/nrm2688.
19. Lee, K.E., Heo, J.E., Kim, J.M., and Hwang, C.S. (2016). N-Terminal Acetylation-Targeted N-End Rule Proteolytic System: The Ac/N-End Rule Pathway. Mol. Cell. *39*, 169–178. https://doi.org/10.14348/molcells.2016.2329.
20. Shemorry, A., Hwang, C.S., and Varshavsky, A. (2013). Control of protein quality and stoichiometries by N-terminal acetylation and the N-end rule pathway. Mol. Cell *50*, 540–551. https://doi.org/10.1016/j.molcel.2013.03.018.
21. Varland, S., Silva, R.D., Kjosås, I., Faustino, A., Bogaert, A., Billmann, M., Boukhatmi, H., Kellen, B., Costanzo, M., Drazic, A., et al. (2023). N-terminal acetylation shields proteins from degradation and promotes age-dependent motility and longevity. Nat. Commun. *14*, 6774. https://doi.org/10.1038/s41467-023-42342-y.
22. Guzman, U.H., Aksnes, H., Ree, R., Krogh, N., Jakobsson, M.E., Jensen, L.J., Arnesen, T., and Olsen, J.V. (2023). Loss of N-terminal acetyltransferase A activity induces thermally unstable ribosomal proteins and increases their turnover in Saccharomyces cerevisiae. Nat. Commun. *14*, 4517. https://doi.org/10.1038/s41467-023-40224-x.
23. Li, Z., Dogra, V., Lee, K.P., Li, R., Li, M., Li, M., and Kim, C. (2020). N-Terminal Acetylation Stabilizes SIGMA FACTOR BINDING PROTEIN1 Involved in Salicylic Acid-Primed Cell Death. Plant Physiol. *183*, 358–370. https://doi.org/10.1104/pp.19.01417.
24. Linster, E., Forero Ruiz, F.L., Miklankova, P., Ruppert, T., Mueller, J., Armbruster, L., Gong, X., Serino, G., Mann, M., Hell, R., and Wirtz, M.

(2022). Cotranslational N-degron masking by acetylation promotes proteome stability in plants. Nat. Commun. *13*, 810. https://doi.org/10.1038/s41467-022-28414-5.

25. Mueller, F., Friese, A., Pathe, C., da Silva, R.C., Rodriguez, K.B., Musacchio, A., and Bange, T. (2021). Overlap of NatA and IAP substrates implicates N-terminal acetylation in protein stabilization. Sci. Adv. *7*, eabc8590. https://doi.org/10.1126/sciadv.abc8590.
26. Arnesen, T., Anderson, D., Torsvik, J., Halseth, H.B., Varhaug, J.E., and Lillehaug, J.R. (2006). Cloning and characterization of hNAT5/hSAN: an evolutionarily conserved component of the NatA protein N-alpha-acetyltransferase complex. Gene *371*, 291–295. https://doi.org/10.1016/j.gene.2005.12.008.
27. Arnesen, T., Starheim, K.K., Van Damme, P., Evjenth, R., Dinh, H., Betts, M.J., Ryningen, A., Vandekerckhove, J., Gevaert, K., and Anderson, D. (2010). The chaperone-like protein HYPK acts together with NatA in cotranslational N-terminal acetylation and prevention of Huntingtin aggregation. Mol. Cell Biol. *30*, 1898–1909. https://doi.org/10.1128/MCB.01199-09.
28. Deng, S., McTiernan, N., Wei, X., Arnesen, T., and Marmorstein, R. (2020). Molecular basis for N-terminal acetylation by human NatE and its modulation by HYPK. Nat. Commun. *11*, 818. https://doi.org/10.1038/s41467-020-14584-7.
29. Van Damme, P., Hole, K., Gevaert, K., and Arnesen, T. (2015). N-terminal acetylome analysis reveals the specificity of Naa50 (Nat5) and suggests a kinetic competition between N-terminal acetyltransferases and methionine aminopeptidases. Proteomics *15*, 2436–2446. https://doi.org/10.1002/pmic.201400575.
30. Deng, S., Magin, R.S., Wei, X., Pan, B., Petersson, E.J., and Marmorstein, R. (2019). Structure and Mechanism of Acetylation by the N-Terminal Dual Enzyme NatA/Naa50 Complex. Structure *27*, 1057–1070.e4. https://doi.org/10.1016/j.str.2019.04.014.
31. Weidenhausen, J., Kopp, J., Armbruster, L., Wirtz, M., Lapouge, K., and Sinning, I. (2021). Structural and functional characterization of the N-terminal acetyltransferase NAA50. Structure *29*, 413–425.e5.
32. Knorr, A.G., Schmidt, C., Tesina, P., Berninghausen, O., Becker, T., Beatrix, B., and Beckmann, R. (2019). Ribosome-NatA architecture reveals that rRNA expansion segments coordinate N-terminal acetylation. Nat. Struct. Mol. Biol. *26*, 35–39. https://doi.org/10.1038/s41594-018-0165-y.
33. Armbruster, L., Linster, E., Boyer, J.-B., Brünje, A., Eirich, J., Stephan, I., Bienvenut, W.V., Weidenhausen, J., Meinnel, T., Hell, R., et al. (2020). NAA50 Is an Enzymatically Active N^{α}-Acetyltransferase That Is Crucial for Development and Regulation of Stress Responses. Plant Physiol. *183*, 1502–1516. https://doi.org/10.1104/pp.20.00222.
34. Weyer, F.A., Gumiero, A., Lapouge, K., Bange, G., Kopp, J., and Sinning, I. (2017). Structural basis of HypK regulating N-terminal acetylation by the NatA complex. Nat. Commun. *8*, 15726. https://doi.org/10.1038/ncomms15726.
35. Gong, X., Huang, Y., Liang, Y., Yuan, Y., Liu, Y., Han, T., Li, S., Gao, H., Lv, B., Huang, X., et al. (2022). OsHYPK-mediated protein N-terminal acetylation coordinates plant development and abiotic stress responses in rice. Mol. Plant *15*, 740–754. https://doi.org/10.1016/j.molp.2022.03.001.
36. Miklánková, P., Linster, E., Boyer, J.B., Weidenhausen, J., Mueller, J., Armbruster, L., Lapouge, K., De La Torre, C., Bienvenut, W., Sticht, C., et al. (2022). HYPK promotes the activity of the N^{α}-acetyltransferase A complex to determine proteostasis of nonAc-X^2/N-degron-containing proteins. Sci. Adv. *8*, eabn6153. https://doi.org/10.1126/sciadv.abn6153.
37. Raychaudhuri, S., Majumder, P., Sarkar, S., Giri, K., Mukhopadhyay, D., and Bhattacharyya, N.P. (2008). Huntingtin interacting protein HYPK is intrinsically unstructured. Proteins *71*, 1686–1698. https://doi.org/10.1002/prot.21856.
38. Faber, P.W., Barnes, G.T., Srinidhi, J., Chen, J., Gusella, J.F., and MacDonald, M.E. (1998). Huntingtin interacts with a family of WW domain proteins. Hum. Mol. Genet. *7*, 1463–1474. https://doi.org/10.1093/hmg/7.9.1463.
39. Raychaudhuri, S., Sinha, M., Mukhopadhyay, D., and Bhattacharyya, N.P. (2008). HYPK, a Huntingtin interacting protein, reduces aggregates and apoptosis induced by N-terminal Huntingtin with 40 glutamines in Neuro2a cells and exhibits chaperone-like activity. Hum. Mol. Genet. *17*, 240–255. https://doi.org/10.1093/hmg/ddm301.
40. Choudhury, K.R., Bucha, S., Baksi, S., Mukhopadhyay, D., and Bhattacharyya, N.P. (2016). Chaperone-like protein HYPK and its interacting partners augment autophagy. Eur. J. Cell Biol. *95*, 182–194. https://doi.org/10.1016/j.ejcb.2016.03.003.
41. Ghosh, D.K., and Ranjan, A. (2022). HYPK coordinates degradation of polyneddylated proteins by autophagy. Autophagy *18*, 1763–1784. https://doi.org/10.1080/15548627.2021.1997053.
42. Gottlieb, L., and Marmorstein, R. (2018). Structure of Human NatA and Its Regulation by the Huntingtin Interacting Protein HYPK. Structure *26*, 925–935.e8. https://doi.org/10.1016/j.str.2018.04.003.
43. Jumper, J., Evans, R., Pritzel, A., Green, T., Figurnov, M., Ronneberger, O., Tunyasuvunakool, K., Bates, R., Žídek, A., Potapenko, A., et al. (2021). Highly accurate protein structure prediction with AlphaFold. Nature *596*, 583–589. https://doi.org/10.1038/s41586-021-03819-2.
44. Zhang, H., Linster, E., Gannon, L., Leemhuis, W., Rundle, C.A., Theodoulou, F.L., and Wirtz, M. (2019). Tandem Fluorescent Protein Timers for Noninvasive Relative Protein Lifetime Measurement in Plants. Plant Physiol. *180*, 718–731. https://doi.org/10.1104/pp.19.00051.
45. Chen, H., Zou, Y., Shang, Y., Lin, H., Wang, Y., Cai, R., Tang, X., and Zhou, J.-M. (2008). Firefly Luciferase Complementation Imaging Assay for Protein-Protein Interactions in Plants. Plant Physiol. *146*, 368–376. https://doi.org/10.1104/pp.107.111740.
46. Bienvenut, W.V., Giglione, C., and Meinnel, T. (2017). SILProNAQ: A Convenient Approach for Proteome-Wide Analysis of Protein N-Termini and N-Terminal Acetylation Quantitation. Methods Mol. Biol. *1574*, 17–34. https://doi.org/10.1007/978-1-4939-6850-3_3.
47. Lin, M.C., Yu, C.J., and Lee, F.J.S. (2022). Phosphorylation of Arl4A/D promotes their binding by the HYPK chaperone for their stable recruitment to the plasma membrane. Proc. Natl. Acad. Sci. USA *119*, e2207414119. https://doi.org/10.1073/pnas.2207414119.
48. Gautschi, M., Just, S., Mun, A., Ross, S., Rücknagel, P., Dubaquié, Y., Ehrenhofer-Murray, A., and Rospert, S. (2003). The yeast N(alpha)-acetyltransferase NatA is quantitatively anchored to the ribosome and interacts with nascent polypeptides. Mol. Cell Biol. *23*, 7403–7414.
49. Evjenth, R.H., Brenner, A.K., Thompson, P.R., Arnesen, T., Frøystein, N.Å., and Lillehaug, J.R. (2012). Human Protein N-terminal Acetyltransferase hNaa50p (hNAT5/hSAN) Follows Ordered Sequential Catalytic Mechanism: COMBINED KINETIC AND NMR STUDY. J. Biol. Chem. *287*, 10081–10088. https://doi.org/10.1074/jbc.M111.326587.
50. Arnesen, T., Van Damme, P., Polevoda, B., Helsens, K., Evjenth, R., Colaert, N., Varhaug, J.E., Vandekerckhove, J., Lillehaug, J.R., Sherman, F., and Gevaert, K. (2009). Proteomics analyses reveal the evolutionary conservation and divergence of N-terminal acetyltransferases from yeast and humans. Proc. Natl. Acad. Sci. USA *106*, 8157–8162. https://doi.org/10.1073/pnas.0901931106.
51. Van Damme, P., Evjenth, R., Foyn, H., Demeyer, K., De Bock, P.J., Lillehaug, J.R., Vandekerckhove, J., Arnesen, T., and Gevaert, K. (2011). Proteome-derived Peptide Libraries Allow Detailed Analysis of the Substrate Specificities of N{alpha}-acetyltransferases and Point to hNaa10p as the Post-translational Actin N{alpha}-acetyltransferase. Mol. Cell. Proteomics *10*, M110 004580. https://doi.org/10.1074/mcp.M110.004580.
52. Callis, J. (2014). The Ubiquitination Machinery of the Ubiquitin System. Arabidopsis Book *12*, e0174. https://doi.org/10.1199/tab.0174.
53. Ma, L., Sun, N., Liu, X., Jiao, Y., Zhao, H., and Deng, X.W. (2005). Organ-Specific Expression of Arabidopsis Genome during Development. Plant Physiol. *138*, 80–91. https://doi.org/10.1104/pp.104.054783.
54. Marshall, R.S., and Vierstra, R.D. (2018). Autophagy: The Master of Bulk and Selective Recycling. Annu. Rev. Plant Biol. *69*, 173–208. https://doi.org/10.1146/annurev-arplant-042817-040606.

55. Song, Z.-T., Chen, X.-J., Luo, L., Yu, F., Liu, J.-X., and Han, J.-J. (2022). UBA domain protein SUF1 interacts with NatA-complex subunit NAA15 to regulate thermotolerance in Arabidopsis. J. Integr. Plant Biol. *64*, 1297–1302.

56. Pechmann, S., Willmund, F., and Frydman, J. (2013). The Ribosome as a Hub for Protein Quality Control. Mol. Cell *49*, 411–421.

57. Tocquin, P., Corbesier, L., Havelange, A., Pieltain, A., Kurtem, E., Bernier, G., and Périlleux, C. (2003). A novel high efficiency, low maintenance, hydroponic system for synchronous growth and flowering of *Arabidopsis thaliana*. BMC Plant Biol. *3*, 2.

58. Wang, C., Shen, L., Fu, Y., Yan, C., and Wang, K. (2015). A Simple CRISPR/Cas9 System for Multiplex Genome Editing in Rice. J Genet Genomics *42*, 703–706. https://doi.org/10.1016/j.jgg.2015.09.011.

59. Lampropoulos, A., Sutikovic, Z., Wenzl, C., Maegele, I., Lohmann, J.U., and Forner, J. (2013). GreenGate - A Novel, Versatile, and Efficient Cloning System for Plant Transgenesis. PLoS One *8*, e83043. https://doi.org/10.1371/journal.pone.0083043.

60. Clough, S.J., and Bent, A.F. (1998). Floral dip: a simplified method for Agrobacterium-mediated transformation of *Arabidopsis thaliana*. Plant J. *16*, 735–743.

61. Edwards, K., Johnstone, C., and Thompson, C. (1991). A simple and rapid method for the preparation of plant genomic DNA for PCR analysis. Nucleic Acids Res. *19*, 1349.

62. Bradford, M.M. (1976). A rapid and sensitive method for the quantitation of microgram quantities of protein utilizing the principle of protein-dye binding. Anal. Biochem. *72*, 248–254.

63. Kong, L., Cheng, J., Zhu, Y., Ding, Y., Meng, J., Chen, Z., Xie, Q., Guo, Y., Li, J., Yang, S., and Gong, Z. (2015). Degradation of the ABA co-receptor ABI1 by PUB12/13 U-box E3 ligases. Nat. Commun. *6*, 8630. https://doi.org/10.1038/ncomms9630.

64. Zhang, H., Quintana, J., Ütkür, K., Adrian, L., Hawer, H., Mayer, K., Gong, X., Castanedo, L., Schulten, A., Janina, N., et al. (2022). Translational fidelity and growth of Arabidopsis require stress-sensitive diphthamide biosynthesis. Nat. Commun. *13*, 4009. https://doi.org/10.1038/s41467-022-31712-7.

65. Bienvenut, W.V., Scarpelli, J.P., Dumestier, J., Meinnel, T., and Giglione, C. (2017). EnCOUNTer: a parsing tool to uncover the mature N-terminus of organelle-targeted proteins in complex samples. BMC Bioinf. *18*, 182. https://doi.org/10.1186/s12859-017-1595-y.

STAR★METHODS

KEY RESOURCES TABLE

REAGENT or RESOURCE	SOURCE	IDENTIFIER
Antibodies		
anti-Beta tubulin	Agrisera	Cat#AS10681; RRID:AB_10754674
anti-Actin	Agrisera	Cat#AS132640; RRID:AB_2722610
anti-Neutravidin-HRP	Invitrogen	Cat#31001
anti-mono- and polyubiquitinylated conjugates recombinant monoclonal antibody-HRP	Enzo life Sciences	Cat#ENZ-ABS840HRP
anti-secondary antibody rabbit IgG-HRP	Agrisera	Cat#AS10852; RRID:AB_10749593
anti-NAA10	Linster et al.[14]	N/A
anti-NAA15	Linster et al.[14]	N/A
Bacterial and virus strains		
E. coli XL1 Blue	Agilent Technologies	Cat#200130-41
BL21 (DE3)	Novagen	Cat#69450
Agrobacterium tumefaciens GV3101	Hölzel biotech	Cat#IG-1082-18
Chemicals, peptides, and recombinant proteins		
Protease inhibitor cocktail	Roche	Cat#11873580001
MG132	Santa-Cruz Biotechnology	Cat#sc-201270
EasyTag™ EXPRESS[35] S Protein Labeling Mix	PerkinElmer	Cat#NEG772007MC
L-azidohomoalanine	Invitrogen	Cat#C10102
Biotin Azide	Invitrogen	Cat#B10185
4-Chlor-7-nitro-benzo-2-oxa-1,3-diazol (NBD-Cl)	Sigma Aldrich	Cat#25455-1G
Proteasome substrate I (Z-Leu-Leu-Leu-AMC)	Sigma Aldrich	Cat#SCP0003-5MG
Luciferin	Promega	Cat#E1602
*Ct*NatA	Weyer et al.[34]	N/A
His6 -*At*HYPK	This study	N/A
His6 -*At*HYPK-cr2	This study	N/A
Critical commercial assays		
HiTrap Chelating High Performance Column	GE Healthcare	Cat#GE17-0408-01
Click-iT™ Protein Reaction Buffer Kit	Invitrogen	Cat#C10276
Fast Gene Scriptase II cDNA Synthesis Kit	NIPPON Genetics	Cat#LS63
qPCRBIO SyGreen Mix Lo-ROX	NIPPON Genetics	Cat#PB20.11–51
FastGene Taq 2x Ready Mix	NIPPON Genetics	Cat#LS27
PCRBIO HiFi Polymerase	NIPPON Genetics	Cat#PB10.41–10
Universal RNA Kit	Roboclon	Cat#E3598
PD SpinTrap G-25 column	Cytiva	Cat#28918004
Deposited data		
N-terminome profiling data	This study	PRIDE: PXD043600 PRIDE: PXD047700
Experimental models: Organisms/strains		
Arabidopsis: Col-0	NASC	CS1092
Arabidopsis: *hypk-3*	NASC	SALK_080671
Arabidopsis: *muse6-1*	Xu et al.[15]	N/A
Arabidopsis: *aminaa15*	Linster et al.[14]	N/A

(*Continued on next page*)

Continued		
REAGENT or RESOURCE	SOURCE	IDENTIFIER
Arabidopsis: *hypk-cr1*	This study	N/A
Arabidopsis: *hypk-cr2*	This study	N/A
Nicotiana benthamiana:	Widely distributed	N/A
Oligonucleotides		
Primers are listed in Tables S4	This study	N/A
Recombinant DNA		
pAtHYPK-Cas9-1	This study	N/A
pAtHYPK-Cas9-2	This study	N/A
pGGZ-HYPK	This study	N/A
pGGZ-nHYPK	This study	N/A
pGGZ-cHYPK	This study	N/A
pGGZ-HYPK-tFT	This study	N/A
pGGZ-HYPK-cr2-tFT	This study	N/A
pGGZ-NAA10	This study	N/A
pCambia1300-HYPK-cr2-nLUC	This study	N/A
pCambia1300-HYPK -nLUC	This study	N/A
pCambia1300-NAA10-nLUC	Miklánková et al.[36]	N/A
pCambia1300-NAA20-nLUC	Miklánková et al.[36]	N/A
pCambia1300-NAA15-cLUC	Miklánková et al.[36]	N/A
pET28a-His6–AtHYPK	This study	N/A
pET28a-His6–AtHYPK-cr2	This study	N/A
Software and algorithms		
GraphPad Prism9	GraphPad	https://www.graphpad.com/
ImageJ	NIH	http://imagej.net/
BioRender	BioRender	https://www.biorender.com/

RESOURCE AVAILABILITY

Lead contact

Further information and requests for resources and reagents should be directed to and will be fulfilled by the lead contact, Markus Wirtz (markus.wirtz@cos.uni-heidelberg.de).

Materials availability

All plant lines and plasmids generated in this study are available from the lead contact upon reasonable request.

Data and code availability

- The N-terminome profiling data are available at the PRIDE repository (https://www.ebi.ac.uk/pride/) with the dataset identifiers PXD043600 and PXD047700
- This paper does not report original code.
- Any additional information required to reanalyze the data reported in this work paper is available from the lead contact upon request.

EXPERIMENTAL MODEL AND STUDY PARTICIPANT DETAILS

Plant materials

This work refers to the Arabidopsis (*Arabidopsis thaliana*) ecotype Columbia-0 (CS1092) as the wild type. The transfer DNA insertion lines *hypk-3* (SALK_080671) were obtained from the Nottingham Arabidopsis Stock Center (www.arabidopsis.info). The NatA-depleted mutant *aminaa15* and *muse6-1* were generated and characterized previously.[15]

Seed germination assays and growth conditions

Plants were germinated and grown on a well-watered turf mixture (Ökohum, Herbertingen) supplemented with 10% [v/v] vermiculite and 2% [v/v] quartz sand. Seeds were stratified for 2 days on humid soil at 4°C in the dark and then transferred to short-day

conditions (8.5-h day, light intensity: 100 μmol m^{-2} s^{-1}; day temperature: 22°C; night temperature: 18°C; relative humidity: 50%) in plant growth chambers (ThermoTec). For seed production or crossing, eight-week-old soil-grown plants were transferred to long-day conditions (16-h light per day; other conditions were the same as in short-day cultivation) and grown until seeds matured in the siliques.

Seeds for hydroponic cultivation were sterilized in 70% ethanol (2 min), followed by a treatment for 10 min in 6% hypochlorite. Seeds were then washed five times with sterile double-distilled H2O (ddH2O) and stratified for 2 days at 4°C in the dark on solid ½ Hoagland solution [2.5 mM $Ca(NO_3)_2$, 0.5 mM $MgSO_4$, 2.5 mM KNO3, 0.5 mM KH_2PO_4, 4 μM Fe-EDTA, 25 μM H_3BO_3, 2.25 μM $MnCl_2$, 1.9 μM $ZnCl_2$, 0.15 μM $CuCl_2$, 50 nM $(NH_4)_6Mo_7O_{24}$, and 0.6% (w/v) microagar (pH 5.8)]. The seedlings were grown in growth cabinets (Percival Intellus, Laborgeräte GmbH) under short-day conditions (8-h light, 120 μmol m^{-2} s^{-1}; day/night temperature: 22°/18°C) for two weeks. Seedlings were then transferred to hydroponic conditions and further grown in a liquid ½ Hoagland solution.[57]

METHOD DETAILS

Constructs for genetic transformation

To generate CRISPR/Cas9 constructs, two single-guide RNAs (sgRNA) targeting the first and second exons of *HYPK* were designed (Table S4) and cloned according to the CRISPR/Cas9 cloning procedure and vectors described in.[58]

To generate complementation constructs, the cDNA sequences encoding for the full-length of *NAA10* or *HYPK* or truncated *HYPK* were amplified using the PCRBIO HiFi Polymerase (PCRBIOSYSTEMS) with specific primers (Table S4). The resulting PCR fragments were cloned into the GreenGate cloning system under the control of the constitutive CaMV 35S promoter.[59] Final vectors were sequenced to confirm sequence identity (EUROFINs) and then stably transformed into *hypk-cr1* plants.

Stable transformation of *A. thaliana* and selection of transgenic plants

Arabidopsis plants were stably transformed with the respective constructs by the established *A. tumefaciens*–mediated floral dip transformation method.[60] Selection of one-week-old soil-grown plants overexpressing *NAA10* or different variants of *HYPK* was performed by spraying glufosinate-ammonium solution (0.2 g/L) three times within 6 days. The surviving plants were genotyped by PCR using specific primers and sequenced to confirm the *hypk-cr1* background (Table S4). Selection of *HYPK* CRISPR/Cas9 plants was performed by applying Hygromycin B (25 mg/L) on ½ MS medium. The surviving plants were sequenced using specific primers to identify mutations (Table S4). The CRISPR/Cas9 construct was eliminated from *hypk-cr1* mutant by selfing. While the CRISPR/Cas9 construct remained in the *hypk-cr2* mutant, probably due to the insertion site being close to the *HYPK* locus.

Extraction of genomic DNA and genotyping

For the PCR-based genotyping of plants, genomic DNA (gDNA) was extracted from leaves as described in Edwards et al..[61] gDNA served as a template for the amplification of distinct alleles with specific primers (Table S4) using the FastGene TAQ Ready Mix PCR Kit (Nippon Genetics). CRISPR-Cas9 induced mutations were confirmed by Sanger sequencing (EUROFINs).

RNA extraction, cDNA synthesis and real-time PCR

Total RNA was extracted from 100 mg of leaf material of soil-grown plants with the Universal RNA Kit (Roboclon). Next, cDNAs were synthesized from total RNA with the Fast Gene Scriptase II cDNA Synthesis Kit (NIPPON Genetics) according to the manufacturer's instructions to generate templates for cloning or real-time PCR. Real-time PCRs were performed according to the manufacturer's instructions with the qPCRBIO SyGreen Mix Lo-ROX (PCR Biosystems) using primer pairs defined in Table S4. The expression levels were normalized to the expression of *PP2A* (*AT1G69960*) or *Actin7* (*At5g09810*) gene.

Protein extraction from Arabidopsis leaf and root tissues

Powdered frozen plant material (0.1 mg for leaves and root) was extracted with 0.4 mL of ice-cold extraction buffer (50 mM HEPES, pH 7.4, 10 mM KCl, 1 mM EDTA, 11 mM EGTA, and 10% [v/v] glycerol) supplemented with 10 mM DTT, 0.5 mM PMSF and 1 x complete protease inhibitor cocktail (Roche) for 15 min on ice. Cell debris were removed by centrifugation (20 min, 20,000 g, 4°C), and the protein concentration in the supernatant was determined according to Bradford.[62]

SDS-PAGE and immunological detection

Extracted proteins were supplemented with 5x-SDS sample buffer (10% SDS, 20% Glycerol, 100 mM Tris pH 7, 0.1% bromophenol blue; 25% 2-mercaptoethanol) and denatured for 10 min at 95°C. Subsequently, proteins were separated by SDS-PAGE and blotted onto PVDF membranes using Mini-Protean II cells (Bio-Rad). Antibodies against NAA10 (1:5,000, Linster et al.[14]), NAA15 (1:5,000), Beta tubulin (1:5,000, Agrisera, AS10681), Actin(1:10,000, Agrisera, AS132640), Neutravidin-HRP (1:100,000, Invitrogen, 31001), mono- and poly-ubiquitination, (1:10,000, Enzo life Sciences, ENZ-ABS840HRP) or the secondary antibody rabbit IgG-HRP (1:25,000, Agrisera, AS10852) were diluted in 1× Tris-buffered saline (50 mM Tris, pH 7.6, 150 mM NaCl, and 0.05% [v/v] Tween 20) supplemented with 0.5% [w/v] BSA. Membranes were developed with the SuperSignal West Dura Extended Duration Substrate (Thermo Scientific). The resulting signals were quantified with the Fiji image processing application.

Subcellular localization and determination of protein stability

The tandem Fluorescence Timer (tFT) system was employed to determine the subcellular localization and protein stability of HYPK and HYPK-cr2 proteins as described previously.[44] In brief, the cDNA sequences encoding for the full-length or truncated *HYPK* were amplified with specific primers (Table S4) and fused upstream of tFT reporter into the GreenGate cloning system.[59] Transient transformation of *Nicotiana benthamiana* leaves and the quantification of the tFT-signal was performed exactly the same way as described in Linster et al..[24]

Firefly luciferase complementation imaging assay

The luciferase complementation imaging assay was performed as described previously.[45] In brief, the cDNA sequences encoding for truncated *HYPK* from *hypk-cr2* mutant were amplified with specific primers (Table S4) and fused upstream of N-Luc in the pCambia-nLuc vector. The resulting vectors were transformed into the *Agrobacterium tumefaciens* strain GV3101. Subsequently, both pCambia-nLuc and pCambia-cLuc vectors containing the respective fusion protein were cotransformed into *Nicotiana benthamiana* leaves as described in Kong et al..[63] After three days, the abaxial sides of leaves were anointed with luciferin (1 mM) and incubated in the dark for 5 min. Subsequently, the luciferase signal was detected with the ImageQuant LAS 4000 at the binning set to 8 × 16 pixels for up 10 min.

Analytical size exclusion chromatography

To test the interaction of the truncated *At*HYPK-cr2 with the NatA complex, the previously described recombinant *Ct*NatA complex was used as recombinant AtNatA was not availbable.[34,36] After cloning of the cDNA encoding for the full length and truncated *At*HYPK-cr2 with specific primers (Table S4) into the pET28a vector, the His6–*At*HYPK and His6–*At*HYPK-cr2 protein were expressed in *Escherichia coli* Rosetta II (DE3) cells. The His6–*At*HYPK and His6-*At*HYPK-cr2 were purified by HiTrap Chelating High Performance Column (GE Healthcare, GE17-0408-01) according to the manufacturer's instructions. A total of 4.5 μM *Ct*NatA was incubated with 45 μM His6-*At*HYPK or His6–*At*HYPK-cr2 at 4°C for 1 h in 20 mM HEPES (pH 8.0) and 250 mM NaCl. Proteins were injected onto a Superdex 200 10/300 GL gel filtration column (GE Healthcare). The differences in the elution profiles of *Ct*NatA, His6-*At*HypK, and the *Ct*NatA-*At*HypK or *Ct*NatA, His6–*At*HYPK-cr2 and the *Ct*NatA-*At*HypK-cr2 mix were analyzed, and proteins in the peak fractions were separated by SDS-PAGE and visualized by Coomassie staining.

Quantification of the drought stress response

Plants were grown on a defined amount of soil for five weeks under short day conditions at 50% humidity (see plant growth conditions). At day 35, watering was stopped for the experimental group, while the control groups were continuously watered. Relative water content of leaves was quantified according to Linster et al..[14] For the drought and re-watering experiments, 9 plants were grown in a single pot filled with the amount of soil under short day conditions. Three-week-old plants were subjected to drought for 18 days and then re-watered for 3 days to calculate survival rate.

Determination of stomatal aperture

Size of stomatal aperture was determined in six-week-old soil-grown plants under short day conditions. For imaging of the stomata, imprints of the abaxial side of three leaves of the same developmental stage were prepared by placing them on a drop of fast-drying glue and applying light pressure. In total, three plants per genotype were used. Imaging was performed with the Leica DM IRB microscope under bright field settings. Data analysis was performed with the Fiji image-processing package.

Determination of proteasome activity

Enzymatic activity of the proteasome was tested in leaves of six-week-old soil-grown plants with the proteasome substrate I (Z-Leu-Leu-Leu-AMC, Sigma-Aldrich) as described in Miklánková et al..[36]

Inhibition of proteasome activity with MG132

To detect polyubiquitinated proteins, the proteasome activity was inhibited by floating leaf discs of six-week-old soil-grown plants on ½ Hoagland medium supplemented with 50 μM MG132 (Santa-Cruz Biotechnology, sc-201270) in the light at 22°C while shaking at 60 rpm. After 6 h, the leaf discs were snap-frozen in liquid nitrogen. Subsequently, proteins were extracted from the plant material and subjected to SDS-PAGE followed by the immunological detection of ubiquitinated proteins with a specific antiserum (1:10,000, Enzo life Sciences, ENZ-ABS840HRP).

Quantification of global translation by isotope labeling

The translation rate in leaves of six-week-old soil-grown plants was quantified by incorporation of radioactively labeled cysteine and methionine using the EasyTag EXPRESS[35] S Protein Labeling Mix (7 mCi, PerkinElmer, Waltham). *In vivo* labeling of proteins and quantification of the incorporated radioactive label was performed as described in Zhang et al.,[64] with the exception that 30μL of the purified protein samples were analyzed.

Detection of newly translated proteins by L-azidohomoalanine labeling

Labeling and detection of newly translated proteins by L-azidohomoalanine was performed according to Linster et al..[14] In brief, leaf discs from six-week-old wild type and *hypk* mutants were incubated for 3 h on ½ Hoagland medium with 50 μM azidohomoalanine. Azidohomoalanine labeled proteins were clicked to Biotin Azide (Invitrogen) using the Click-iT Protein Reaction Buffer Kit (Invitrogen) and detected with the specific Neutravidin-HRP (1:100,000, Invitrogen, 31001). DMSO treated wild-type leaf discs were used as a control to show endogenous biotinylated proteins.

Determination of free N terminus levels

The amount of free N-termini was determined in the protein fraction of foliar proteins extracted from six-week-old soil grown plants after specific staining with 4-Chlor-7-nitro-benzo-2-oxa-1,3-diazol (0.5 mM, Sigma Aldrich, synonymous to NBD-Cl). Labeling of proteins and quantification of the fluorescence signal was performed according to Linster et al..[14] PD SpinTrap G-25 column (Cytiva) was used to remove free amino acids and other low-molecular-weight components from the soluble protein fraction.

Quantification of the N-terminal acetylome

The N-acetylome of proteins extracted from leaves of six-week-old soil-grown plants or leaves and roots of five-week-old hydroponically grown plants was determined with the SILProNAQ approach.[46] Briefly, plant materials were frozen and ground, and resuspended in a specific buffer (50 mM HEPES/NaOH pH 7.2, 1.5 mM MgCl2, 1 mM EGTA, 10% Glycerol, 1% Triton, 2mM PMSF, 150 mM NaCl, protease inhibitor cocktail tablet) for protein extraction. The free N-termini were labeled with d_3-Acetyl groups, then the proteins were digested with trypsin and the resulting peptides were fractionated using SCX chromatography. N-terminally enriched peptide fractions were then analyzed by LC-MS/MS on an LTQ-Orbitrap Velos, and the data files were processed for identification and quantification with Mascot Distiller, followed by the application of the EnCOUNTEr parsing tool.[65]

Cell-free protein degradation assay

Leaf materials from six-week-old soil-grown plants under short day condition were harvested and ground to fine powder. The soluble proteins were extracted on ice for 20 min by adding two volumes of *in vitro* degradation buffer (25 mM Tris–HCl [pH 7.5], 10 mM NaCl, 10 mM MgCl2, 4 mM PMSF, 5 mM dithiothreitol, and 10 mM ATP). Supernatants were cleared by centrifugation at 20,000 g for 20 min at 4°C, and incubated at 22°C for indicated time. Supernatants treated with 50 mM MG132 (Santa-Cruz Biotechnology, sc-201270) served as negative controls. The degradation assay was terminated by adding SDS–PAGE sample buffer and the protein amount was quantified by immunological detection with specific antisera.

Prediction of protein structure

Structure prediction of *At*HYPK was generated by AlphaFold2.[43]

QUANTIFICATION AND STATISTICAL ANALYSIS

Data in figures was expressed as mean ± SEM. Replicates in different experiments were stated in corresponding Figure legends. Statistical analyses were performed with GraphPad Prism9. When two groups were compared, an unpaired two-tailed Student's t-test was used. Significant differences are indicated with asterisks (*$p < 0.05$ or **$p < 0.01$). When comparing more than two groups, a pairwise multiple comparisons with a one-way ANOVA followed by a Tukey's test was performed. Significant differences between groups are indicated with different letters.

Accession numbers

Sequence data from this article can be found in TAIR under Arabidopsis Genome Initiative accession numbers AT3G06610 (*At*HYPK), AT5G13780 (*At*NAA10) and AT1G80410 (*At*NAA15).

Cell Reports, Volume *43*

Supplemental information

HYPK controls stability and catalytic activity of the N-terminal acetyltransferase A in *Arabidopsis thaliana*

Xiaodi Gong, Jean-Baptiste Boyer, Simone Gierlich, Marlena Pożoga, Jonas Weidenhausen, Irmgard Sinning, Thierry Meinnel, Carmela Giglione, Yonghong Wang, Rüdiger Hell, and Markus Wirtz

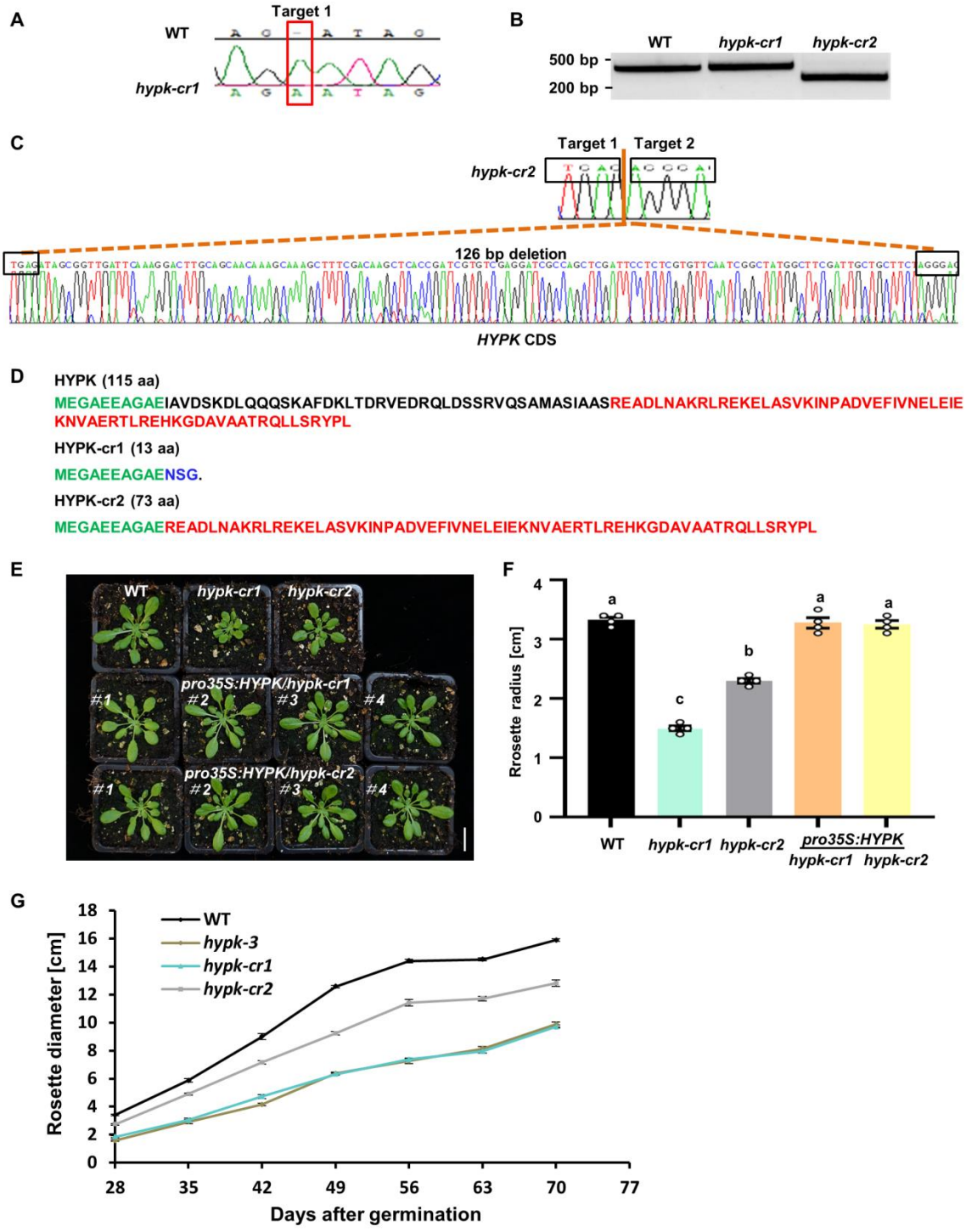

Supplementary Figure S1: Verification of *hypk-cr1* and *hypk-cr2* mutants and growth rates of wild type and *hypk* mutants.

(**A**) Sequencing of the *HYPK* gene in the *hypk-cr1* mutant uncovers the introduction of adenine at position 31 downstream of the start ATG. (**B**) RT-PCR amplification of the *HYPK* mRNAs in the wild type (WT) and the CRISPR-Cas9 *hypk* mutant reveals the truncated mRNA in *hypk-cr2*. (**C**) Sequencing of the *HYPK* mRNA in the *hypk-cr2* mutant uncovers the absence of 126 bp in the HYPK CDS encoding for 42 amino acids. (**D**) Protein sequence of the wild-type HYPK (115 aa) and the HYPK-cr1 and HYPK-cr2 proteins translated in the respective CRISPR-Cas9 mutants. Green indicates the portion of the

wild type HYPK protein expressed in *hypk-cr1*. The protein sequence deleted in the HYPK-cr2 protein is shown in black in the wild type HYPK sequence. The red color displays the C-terminal part of HYPK that is fused to the HYPK N-terminus in the HYPK-cr2 protein. Blue indicates non-sense amino acids translated due to the mutation in the *hypk-cr1* mutant. (**E** and **F**) Phenotype (**E**) and rosette radius (**F**) of five-week-old soil-grown wild type (WT), *hypk-cr1* and *hypk-cr2* and transgenic lines complemented with the full-length HYPK. Data are shown as means ± SEM. Different letters indicate individual groups identified by pairwise multiple comparisons with a one-way ANOVA followed by a Tukey´s test ($P < 0.05$, $n = 4$). Scale bar = 2 cm. (**G**) The rosette diameter of wild type plants and *hypk* mutants grown on soil under short-day conditions (100 µE, 8.5 hours light, temperature: 22°C / 18°C, humidity 50%) were determined as a proxy for growth at the indicated time points. Data are shown as means ± SEM ($n = 10$ individuals).

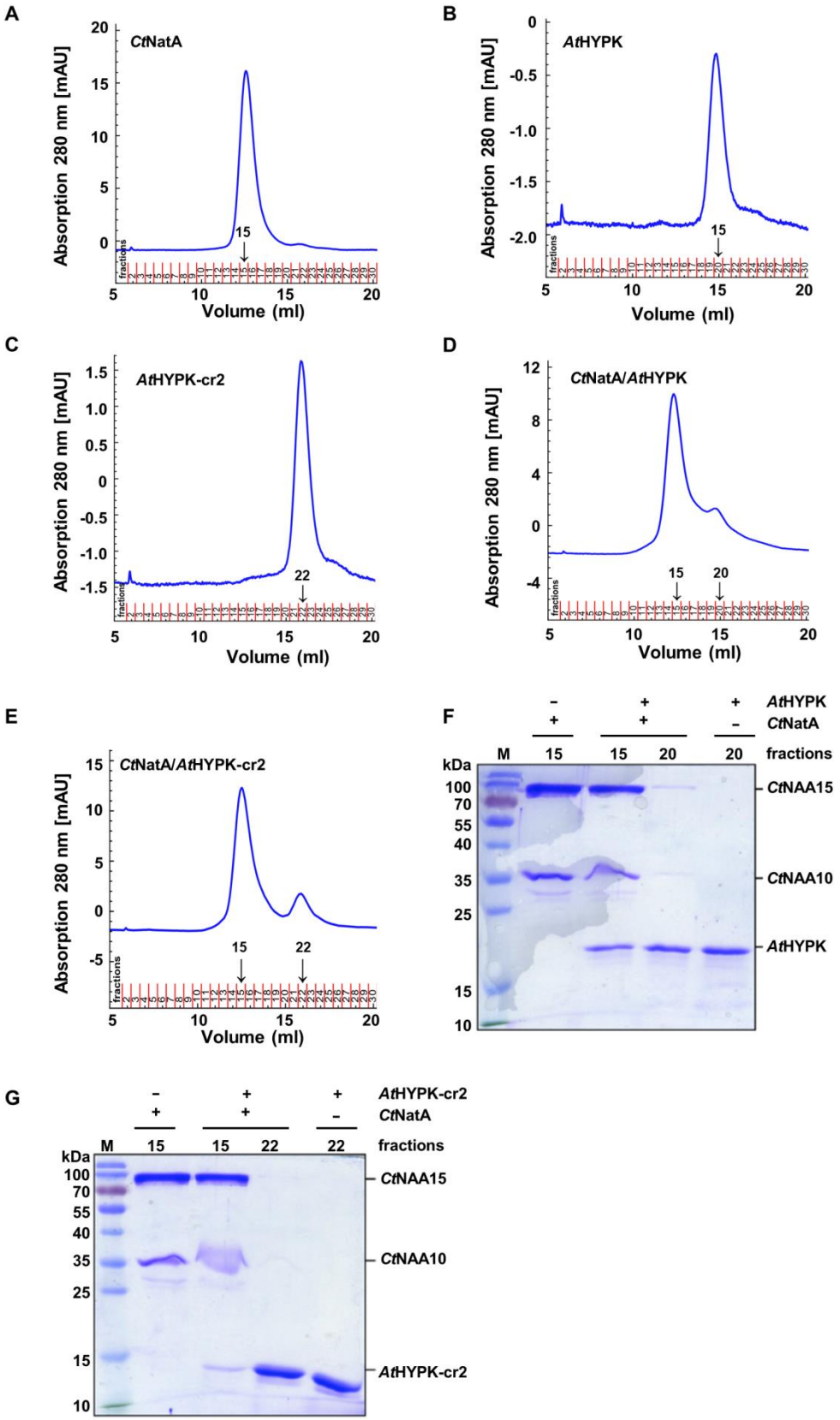

Supplementary Figure S2: Size-exclusion chromatography and SDS-PAGE analysis of *At*HYPK or *At*HYPK-cr2 in complex with *Ct*NatA.

(**A**-**E**) Chromatograms of the analytical size-exclusion chromatography of *Ct*NatA (**A**), *At*HYPK (**B**), *At*HYPK-cr2 (**C**), and mixtures of *Ct*NatA with *At*HYPK (**D**) or HYPK-cr2 (**E**). Proteins were separated using a Superdex200 10/300GL column with a flow rate of 1 ml min^{-1}. Fractions of different sizes were collected during the protein separation (see x-axes). (**F** and **G**) The fractions corresponding to distinct protein peaks (indicated by arrows, fraction size: 0.5 ml) in the chromatogram were analyzed by SDS-PAGE. Separation of the *Ct*NatA-*At*HYPK complex and its components (**F**) or the *Ct*NatA-*At*HYPK-cr2 and its components (**G**) by SDS-PAGE. Fractions corresponding to the high-molecular-weight complexes (fraction 15, either *Ct*NatA or *Ct*NatA + *At*HYPK variants) or the *At*HYPK variants (fraction 20 for *At*HYPK and fraction 22 for *At*HYPK-cr2) were stained with Coomassie brilliant blue after SDS PAGE separation. The physical interaction of both *At*HYPK variants with *Ct*NatA is demonstrated by finding both protein variants in the protein fraction also containing *Ct*NatA.

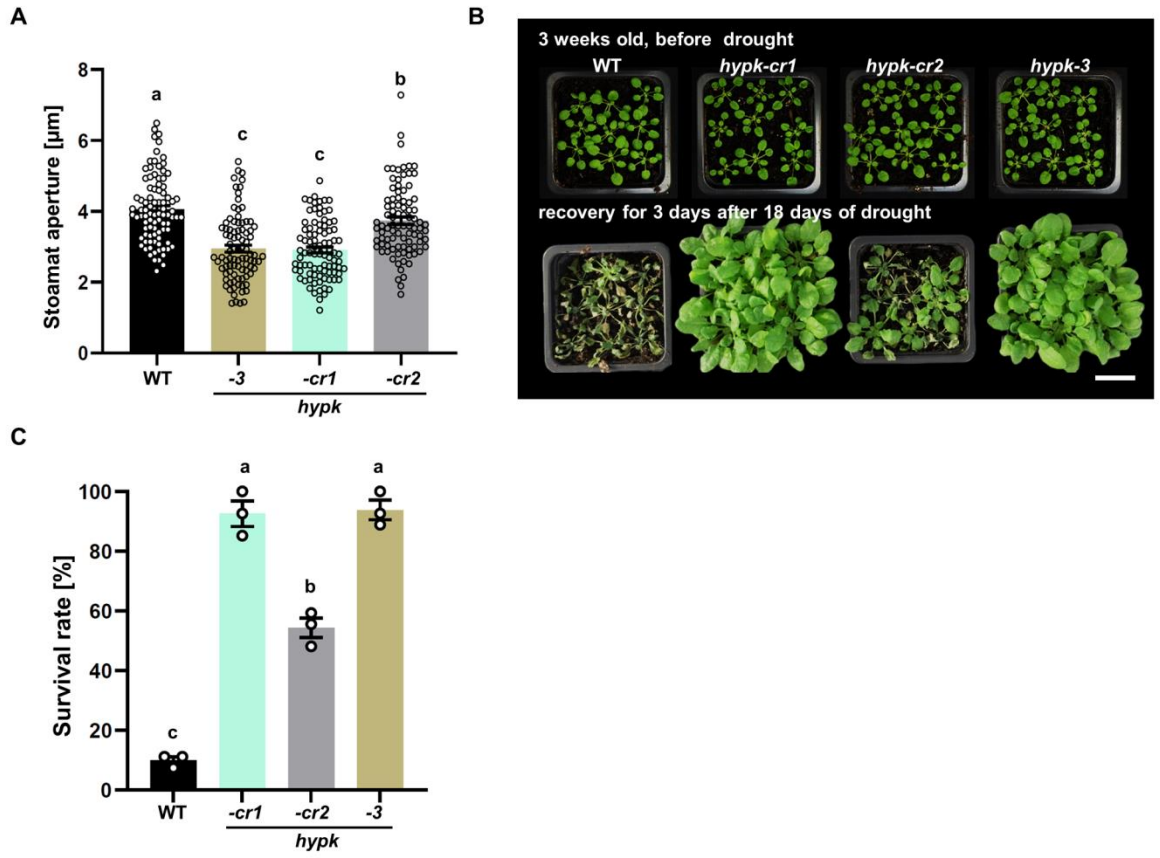

Supplementary Figure S3. The *hypk* mutants have decreased stomatal apertures and are more resistant to soil drying.

(**A**) Quantification of the stomatal aperture from epidermal imprints of WT, *hypk-3*, *hypk-cr1* and *hypk-cr2* grown on soil for six weeks under sufficient water supply. Representative images of of stomata are shown in Figure 2C. Data are shown as means ± SEM (n = 90). Circles indicate data points. Different letters indicate individual groups identified by pairwise multiple comparisons with a one-way ANOVA followed by a Tukey´s test ($P < 0.05$). (**B**) Representative phenotypes of soil-grown wild type (WT) and *hypk* mutants before (three-week-old) and after recovery for 3 days after 18 days of drought treatment. Plants were grown on soil under short-day conditions. Scale bar = 2 cm. (**C**) The survival rate of wild type (WT) and *hypk* mutants after drought treatment. Nine plants were grown in a single pot and three pots were grouped to calculate survival rates, a total of 81 plants were tested. Data are shown as means ± SEM (n = 3). Circles indicate data points. Different letters indicate individual groups identified by pairwise multiple comparisons with a one-way ANOVA followed by a Tukey´s test ($P < 0.05$).

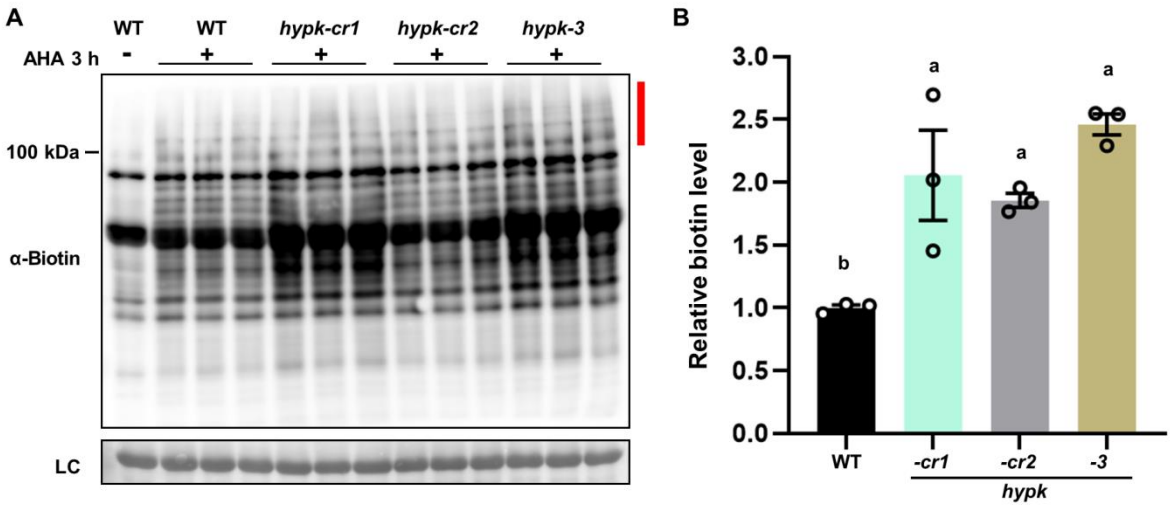

Supplementary Figure S4. Comparison of azidohomoalanine incorporation into foliar proteins of wild type and *hypk* mutants.

Newly translated proteins were labeled with 50 µM azidohomoalanine (AHA) by floating leaf discs of six-week-old wild type (WT) and *hypk* mutants for 3 h on ½ Hoagland medium. Azidohomoalanine incorporation into proteins derived from wild type (WT) and *hypk* leaves was detected (**A**) and quantified (**B**) after azidohomoalanine-mediated biotin labeling and immunoblotting with the specific Neutravidin-HRP (1:100,000, Invitrogen, 31001). DMSO treated wild-type leaf discs were used as a control to show endogenous biotinylated proteins. The red bar indicates the area of the western blot used for quantification, which did not contain any endogenous biotinylated proteins . Amido black staining of proteins transferred to the PVDF membrane served as loading control (LC). Data are shown as means ± SEM (n = 3). Circles indicate individual data points. Different letters indicate individual groups identified by pairwise multiple comparisons with a one-way ANOVA followed by a Tukey´s test ($P < 0.05$).

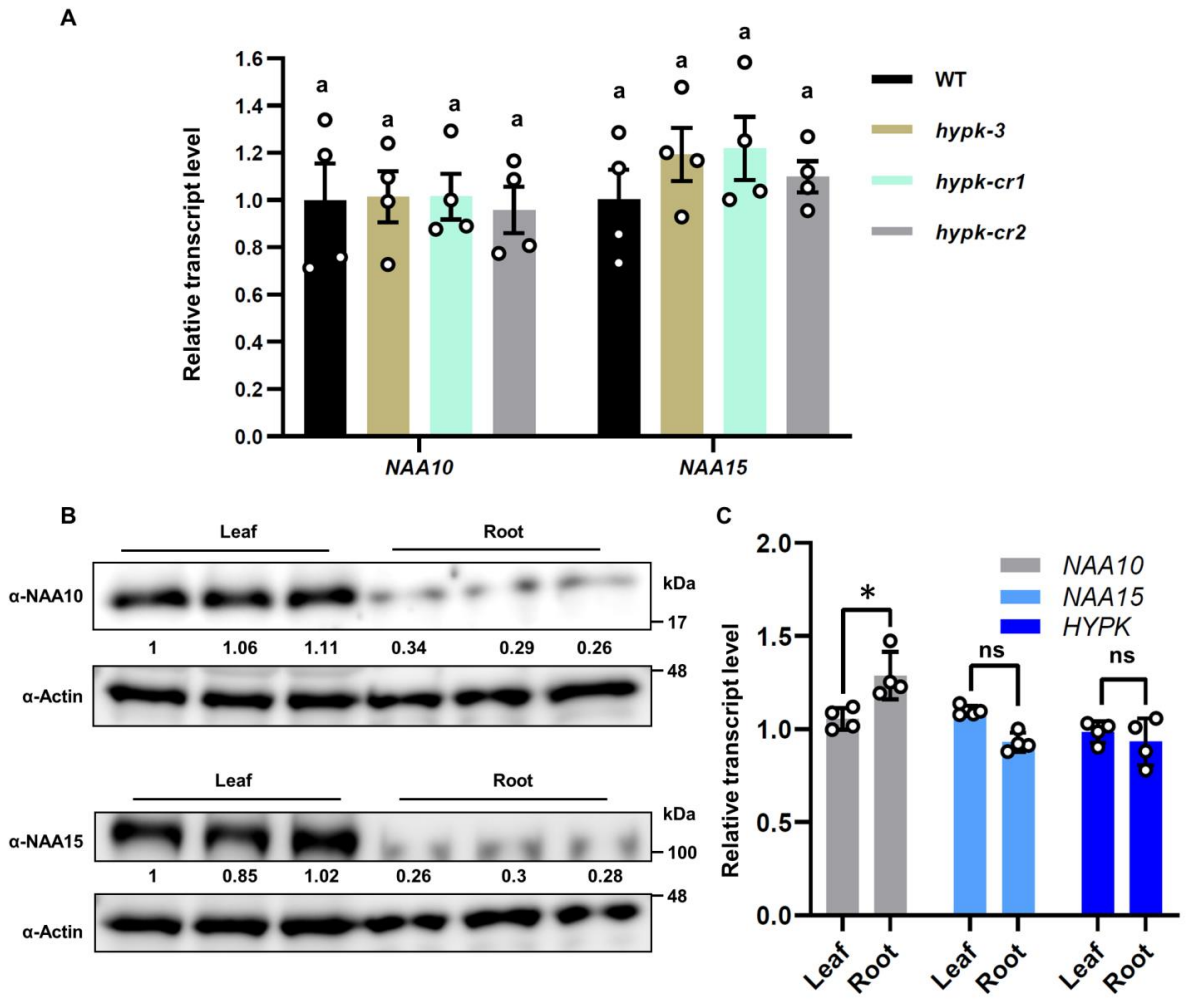

Supplementary Figure S5: Steady-state levels of *HYPK* transcripts, and transcripts and proteins of NatA core subunits in leaves and roots.

(**A**) Steady-state transcript levels of *NAA10* and *NAA15* were determined in leaves of six-week-old soil-grown wild type (WT, black), *hypk-3* (ocher), *hypk-cr1* (light green), and *hypk-cr2* (grey) by qRT-PCR using specific primers (Table S4). *PP2A* served as the reference genes used for normalization. Data are shown as means ± SEM (n = 4). Circles indicate data points. Different letters indicate individual groups identified by pairwise multiple comparisons with a one-way ANOVA followed by a Tukey´s test ($P < 0.05$). (**B**) Immunological detection of NAA10 and NAA15 protein levels in leaves and roots of six-week-old hydroponically grown wild type. Actin served as an internal control. Numbers below the immunological detection indicate the abundance of the respective protein species relative to the signal in replicate one after internal normalization to Actin. (**C**) The transcript levels of *NAA10* (gray), *NAA15* (light blue) and *HYPK* (dark blue) were determined in leaves and roots of six-week-old hydroponically grown wild type by qRT-PCR using specific primers (Table S4). *Actin7* (*At5g09810*) served as the reference genes used for normalization. Data are shown as means ± SEM (n = 4). Circles indicate data points. Significance was determined by two-sided Student's *t*-test in GraphPad Prism 9.0. ∗$P < 0.05$, ns, no significance.

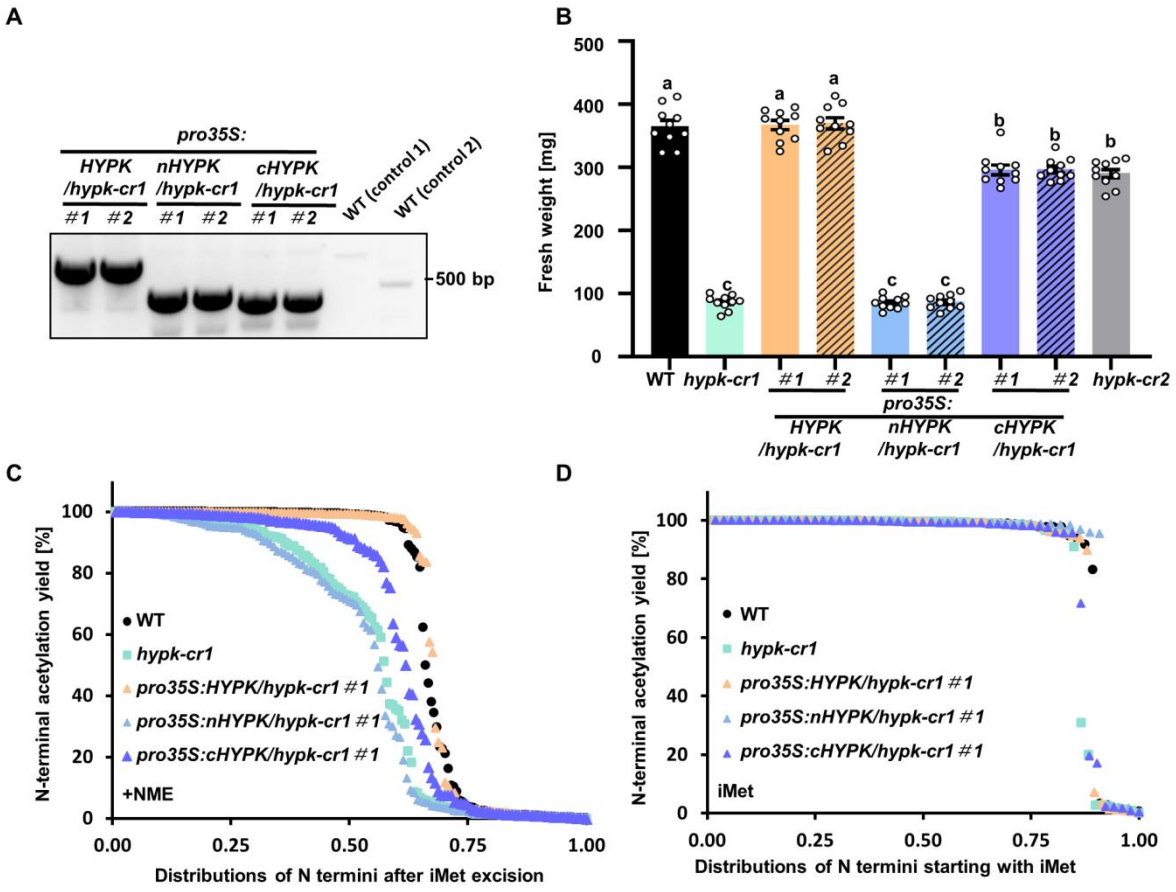

Supplementary Figure S6: Characterization and N-terminome profiling of *hypk-cr1* plants complemented with the full-length or truncated HYPK driven by 35S promoter.

(**A**) PCR-based genotyping of transgenic plants complemented with the full-length HYPK, the HYPK N-terminus (nHYPK) or the UBA domain of HYPK (cHYPK) using specific primers (Table S4). Wild type (WT) negative control 1 showed the specificity of primer pair (35S pro F & HYPK R) used for amplifying fragments from transgenic plants complemented with the full-length HYPK or cHYPK. WT control 2 served as a negative control for primer pair (35S pro F & nHYPK R) used to amplify a *pro35S:nHYPK* specific DNA fragment in transgenic plants. (**B**) The rosette fresh weight of five-week-old wild type (WT, black), *hypk-cr1* (light green), *hypk-cr2* (grey) and *hypk-cr1* complemented with the full-length HYPK (ocher), the HYPK N-terminus (nHYPK, light blue) or the UBA domain of HYPK (cHYPK, light purple) was determined as a proxy for growth. Plants were grown on soil under short-day conditions. Data are shown as means ± SEM (n = 10). Circles indicate data points. Different letters indicate individual groups identified by pairwise multiple comparisons with a one-way ANOVA followed by a Tukey´s test ($P < 0.05$). (**C** and **D**) Distribution for N-terminal acetylation yields of predicted NatA substrates (**C**) and N-termini starting with the iMet (**D**) in leaves of wild type (WT, black), *hypk-cr1* (light green) and *hypk-cr1* complemented with the full-length HYPK (ocher), the HYPK N-terminus (nHYPK, light blue) or the UBA domain of HYPK (cHYPK, light purple) as determined by the SILProNAQ mass-spectrometry approach.

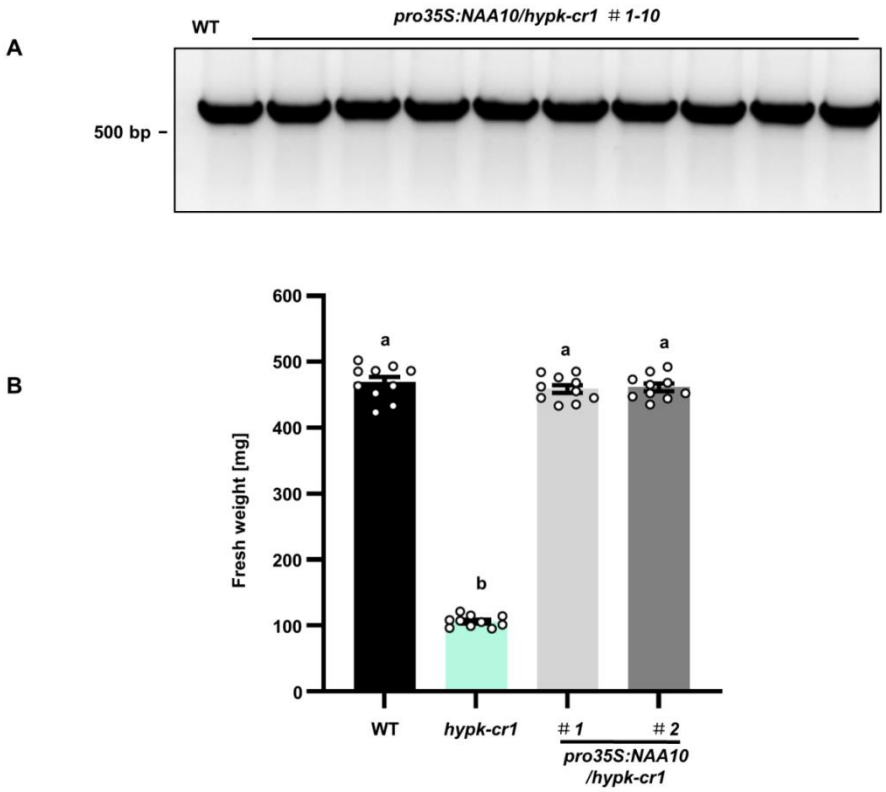

Supplementary Figure S7: Expression of NAA10 rescues the *hypk-cr1* phenotype.

(**A**) PCR-based genotyping of NAA10 overexpressing plants in *hypk-cr1* background using specific primers (Table S4). Wild type (WT) served as a negative control. (**B)** The rosette fresh weight of six-week-old wild type (WT, black), *hypk-cr1* (light green), and two *hypk-cr1* lines complemented with the full-length NAA10 (#1 light grey, #2 dark grey), was determined as a proxy for growth. Plants were grown on soil under short-day conditions. Data are shown as means ± SEM (n = 10). Circles indicate data points. Different letters indicate individual groups identified by pairwise multiple comparisons with a one-way ANOVA followed by a Tukey´s test ($P < 0.05$)

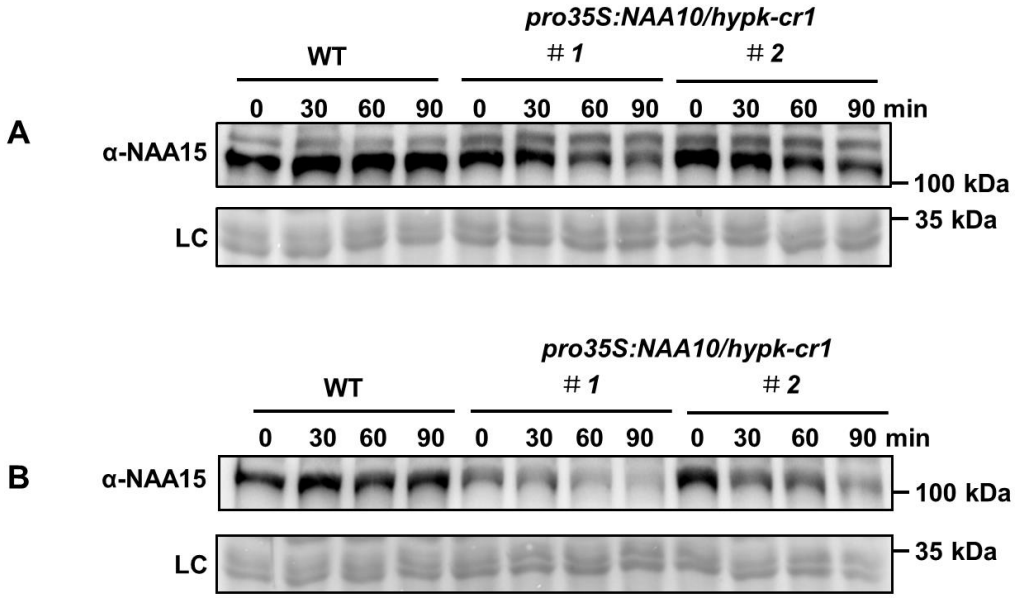

Supplementary Figure S8: Independent repetitions of the cell-free degradation assays for NAA15 in wild type and *pro35S:NAA10/hypk-cr1* lines.

Quantification of NAA15 degradation rate in the leaves of wild type (WT) and two *hypk-cr1* lines complemented with NAA10 by a cell-free degradation assay. The degradation rate is based on the immunological detection of NAA15 at the indicated time points with specific antisera (α-NAA15) as described in the material and methods. Amido black staining of proteins transferred to the PVDF membrane served as loading control (LC). Two independent repetitions with leaf extracts from individual plants are shown in (**A**) and (**B**).

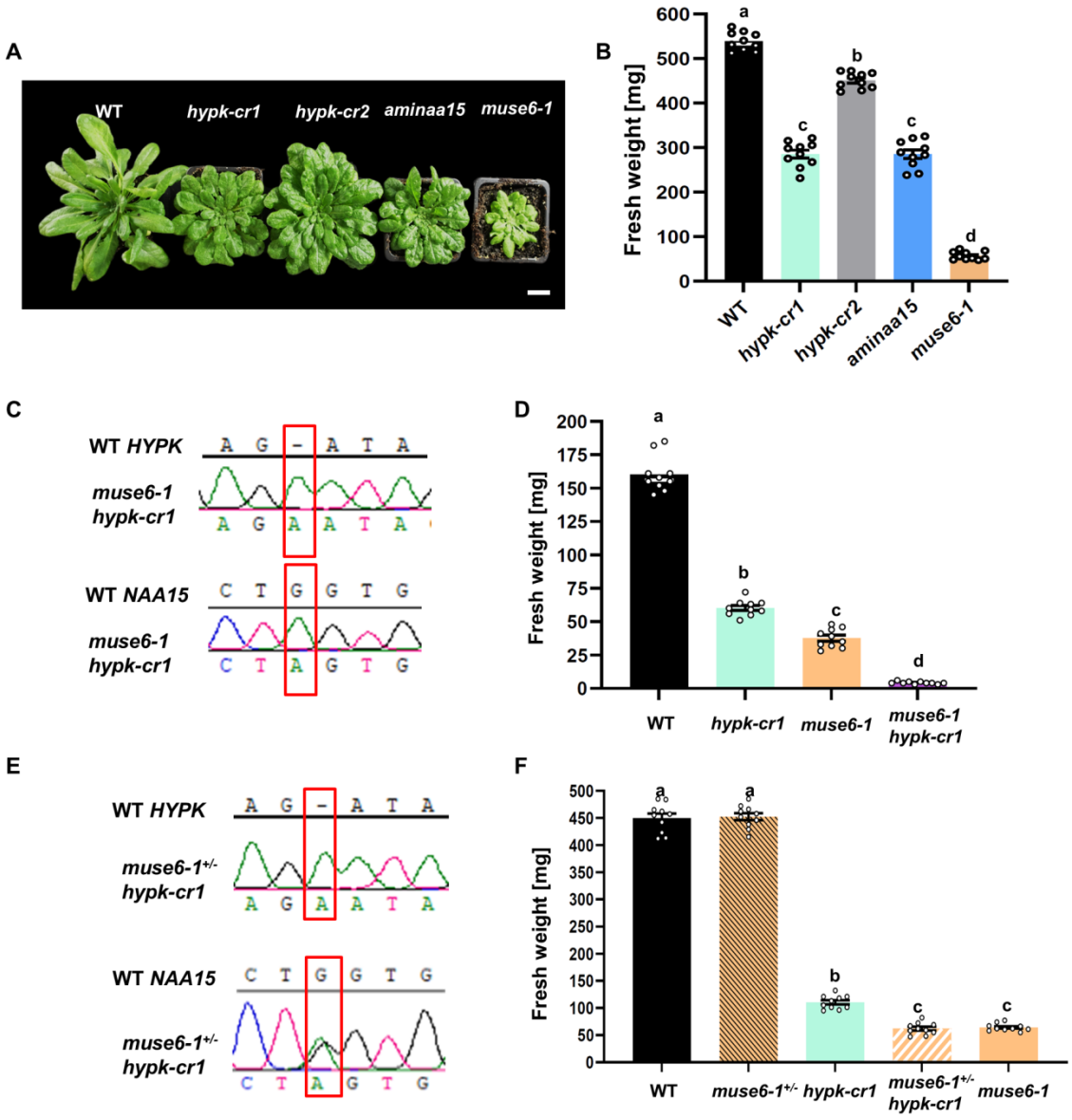

Supplementary Figure S9: Phenotypic analysis of wild type, *hypk* and *NAA15*-depleted mutants, and characterization of the *muse6-1*$^{+/-}$ *hypk-cr1* double mutant and its parental lines.

(**A**) Phenotype of eight-week-old soil-grown wild type (WT), *hypk-cr1*, *hypk-cr2,* and the NAA15-depleted mutants: *aminaa15* and *muse6-1*. Scale bar = 2 cm. (**B**) The rosette fresh weight of eight-week-old wild type (black), *hypk-cr1* (light green), *hypk-cr2* (gray), and the NAA15-depleted *aminaa15* (blue) and *muse6-1* (ocher) mutants. Plants were grown on soil under short-day conditions. Data are shown as means ± SEM (n = 10). Circles indicate data points. Different letters indicate individual groups identified by pairwise multiple comparisons with a one-way ANOVA followed by a Tukey´s test ($P < 0.05$). (**C**) Sequencing of the *HYPK* and the *NAA15* gene in the *muse6-1 hypk-cr1* double mutants confirms the homozygosity of both alleles. (**D**) The rosette fresh weight of four-week-old wild type (WT, black), *hypk-cr1* (light green), *muse6-1* (ocher), and the *muse6-1 hypk-cr1* double (grey) was determined as a proxy for growth. Plants were grown on soil under short-day conditions. Data are shown as means ± SEM (n = 10). Circles indicate data points. Different letters

indicate individual groups identified by pairwise multiple comparisons with a one-way ANOVA followed by a Tukey´s test ($P < 0.05$). (**E**) Sequencing of the *HYPK* and the *NAA15* gene in the *muse6-1*$^{+/-}$ *hypk-cr1* double mutants confirms the heterozygosity of the *NAA15* and the homozygosity of the *HYPK* allele. (**F**) The rosette fresh weight of six-week-old wild type (WT, black), heterozygous *muse 6-1* (*muse6-1*$^{+/-}$, black dashed ocher), *hypk-cr1* (light green), the *muse6-1*$^{+/-}$ *hypk-cr1* double (white dashed ocher) and *muse6-1* (ocher) was determined as a proxy for growth. Plants were grown on soil under short-day conditions. Data are shown as means ± SEM (n = 10). Circles indicate data points. Different letters indicate individual groups identified by pairwise multiple comparisons with a one-way ANOVA followed by a Tukey´s test ($P < 0.05$).